THE ASTROPHYSICAL JOURNAL SUPPLEMENT SERIES, 132:37–71, 2001 January

OPTICAL CLASSIFICATION OF SOUTHERN WARM INFRARED GALAXIES

L. J. KEWLEY, C. A. HEISLER,[1] AND M. A. DOPITA
Research School of Astronomy and Astrophysics, Australian National University, Private Bag, Weston Creek PO, ACT 2611, Australia; lkewley@mso.anu.edu.au, mad@mso.anu.edu.au

AND

S. LUMSDEN
Anglo-Australian Observatory, P.O. Box 296, Epping, NSW 1710, Australia
Received 2000 May 20; accepted 2000 August 23

ABSTRACT

In this paper, we present high-resolution optical spectra and optical classifications from our large sample of 285 warm infrared galaxies $10^8 < L_{IR} < 10^{12.5}\ L_\odot$. We have classified these galaxies using new theoretical lines on the standard optical diagnostic diagrams. We use a theoretical extreme mixing line between the starburst and AGN regions to classify LINER galaxies and we define a theoretical boundary separating AGNs from starbursts. We find that many galaxies previously classified as LINERs appear to lie on a mixing sequence between starburst and AGN type galaxies. These are likely to be of a composite nature with their excitation being a combination of photoionization due to hot stars plus either ionization by a power-law radiation field associated with an AGN or shock excitation where the shock may result from such processes as cooling flows, superwind activity, or an accretion disk around an AGN. We compare our theory-based classification scheme with the previous semiempirical scheme of Veilleux & Osterbrock . We find that our classification method results in 6% ambiguity in classifications between the different diagnostic diagrams compared with 16% ambiguity using the traditional Veilleux & Osterbrock method. We find that 70% of the galaxies in our sample are classified optically as starburst, 17% are Seyfert 2, 4% are Seyfert 1, and 0.4% are LINERs. A further 2% of our sample are certainly composite galaxies. A fraction (20%) of the Seyfert galaxies, 3% of the starburst galaxies, and 71% of the ambiguous galaxies are possibly composite in nature (11% of the total sample).

Subject headings: galaxies: active — galaxies: fundamental parameters — galaxies: ISM — galaxies: starburst — infrared: galaxies — techniques: spectroscopic

On-line material: machine-readable tables

1. INTRODUCTION

Since their discovery by Rieke & Low (1972), infrared galaxies—galaxies dominated by their infrared (IR) luminosity—have been studied heavily to determine the source of their large infrared flux. They derive their power from either rapid star formation or an active nucleus or a combination of the two. Despite numerous studies in the area, the nature of their ultimate energy source is still a vigorous issue of debate. The *Infrared Astronomical Satellite* (*IRAS*), launched in 1983, revolutionized the study of infrared galaxies by revealing a large population of such galaxies.

Infrared galaxies are classed according to their infrared luminosity L_{IR}. The ultraluminous infrared galaxies are generally defined as those with $L_{IR} > 10^{12}\ L_\odot$, while the luminous infrared galaxies (LIRGs) are classed as those with $L_{IR} > 10^{11}\ L_\odot$. The galaxies in the sample described here cover a wider luminosity range of $10^8 < L_{IR} < 10^{12.5}\ L_\odot$. The majority of the lower luminosity *IRAS* galaxies have been shown to be powered predominantly by star formation (Veilleux et al. 1995). Similarly, some investigations reveal that ultraluminous infrared galaxies are also dominated by star formation (Genzel et al. 1998). It is therefore likely that the ultraluminous infrared galaxies represent extreme cases of star formation activity. In contrast, it has been found that the incidence of AGNs detected with optical spectra increases with infrared luminosity, with more than 50% of ultraluminous ($L_{IR} > 10^{12.3}$) infrared galaxies being classed as AGNs in the study by Veilleux, Kim, & Sanders (2000) (see also Sanders et al. 1988a; Veilleux et al. 1995; Kim, Veilleux, & Sanders 1998). Many of these AGN-type galaxies have warmer infrared colors. Complicating the diagnosis of the energy source of infrared galaxies are composite galaxies, containing both starburst and AGN activity (e.g., Mazzarella et al. 1994; Genzel et al. 1998). Deep infrared imaging has shown that many of these types of galaxies contain rings of circumnuclear star formation close to the nucleus (see, e.g., Mazzarella et al. 1994; Bransford et al. 1998; Scoville et al. 2000). The detailed relationship, if any, between starburst and AGN activity in these composite systems is either poorly understood or unknown. Evolutionary scenarios have been proposed such as that by Sanders et al. (1988b) in which the tidal interactions caused by two merging galaxies induce star formation and subsequently activate an AGN within the merged galaxy. The purpose of our warm infrared galaxy project is to determine whether such an evolutionary sequence exists for these galaxies.

Spectroscopic studies have, in the past, proved a useful tool for determining the power source in active galaxies. The classification of the dominant energy source in emission line galaxies by optical spectral diagnostics was first proposed by Baldwin, Phillips, & Terlevich (1981), and the classification scheme was revised and extended by Osterbrock & de Robertis (1985) and Veilleux & Osterbrock (1987, hereafter VO87). These revised diagnos-

[1] This paper is dedicated to the memory of Charlene A. Heisler (deceased, 1999 October 28), whose enthusiasm and dedication were a major driving force behind this project.

tics are used here with new theoretical diagnostic lines. For both schemes, the line diagnostic tools are based on emission-line intensity ratios. Galaxies may be separated using this method into the categories of narrow-line AGNs and H II region–like galaxies because of the differing nature of the photoionization source. AGNs are photoionized by nonthermal or power-law continua (Koski 1978) or by fast shocks (Dopita & Sutherland 1995), while H II region–like galaxies are ionized by hot stars (Huchra 1977). Narrow-line radio-quiet AGNs can be divided into two groups: low-ionization narrow emission line region galaxies (LINERs) and Seyferts. Like Seyferts, LINERs may be photoionized by power-law continua (Veilleux & Osterbrock 1987) or alternatively they may be shock excited (Dopita et al. 1997a; Lutz, Veilleux, & Genzel 1999). The LINERS, as their name implies, are dominated by the emission lines of species of low ionization. Using excitation dependant line ratio diagnostic diagrams therefore, it is easy to distinguish between the three main types of narrow emission line galaxies; Seyfert galaxies, starburst galaxies, and LINERs.

In order to determine the dominant power source in infrared galaxies, and the connection (if any) between their starburst and AGN activity, we have selected a large sample of 285 *IRAS* galaxies for optical spectroscopy. These cover a wide range of infrared luminosities ($8.0 < \log(L_{IR}) < 12.5$). The spectroscopic results of this sample are the subject of this paper. The full spectroscopic data and classification method are given in §§ 3 and 4, respectively, results are presented in § 5, and our summary is given in § 6.

2. SAMPLE SELECTION

Our sample consists of 285 *IRAS* galaxies south of decl. $= +10°$ selected from the catalog by Strauss et al. (1992). In addition to the criteria already imposed by Strauss et al., our sample satisfies the following additional criteria:

1. Flux at 60 μm > 2.5 Jy with moderate or high quality detections at 25, 60, and 100 μm.
2. Redshift < 8000 km s^{-1} for $\log(L_{FIR}) < 11$ and $< 30{,}000$ km s^{-1} for $\log(L_{FIR}) > 11$.
3. Galactic latitude $|b| > 15°$, and declination $\delta < 0°$.
4. Warm FIR colors; $8 > F_{60}/F_{25} > 0.5$ and $2 > F_{60}/F_{100} > 0.5$.

Here F_{25}, F_{60}, and F_{100} are the *IRAS* fluxes at 25, 60, and 100 μm, respectively.

Many studies of *IRAS* selected active galaxies have focussed on galaxies which satisfy the "warm" selection criterion: $F_{60}/F_{25} < 5$. This warm selection criterion was developed by Miley, Neugebauer, & Soifer (1985), who used it to successfully select for Seyfert galaxies. Carter (1984) and de Grijp et al. (1992) both obtained optical spectra of warm *IRAS* objects. Carter found 77% of his objects to be Seyferts, and de Grijp et al. found 70% of their objects to be Seyferts, confirming the strong selection of Seyfert galaxies according to the warm selection criterion.

Recently, it has been shown that the detectability of polarized broad-line emission depends on FIR colors, such that Seyferts with warm FIR colors preferentially have broad-line emission when viewed by spectropolarimetry (Heisler, Lumsden, & Bailey 1997). Other evidence for hidden broad-line activity observed for warm galaxies has been found in studies using near infrared spectroscopy (e.g., Young et al. 1996; Veilleux, Goodrich, & Hill 1997). Since the dust temperature depends on the local radiation field, the warm selection criteria is also likely to select for galaxies having more concentrated star formation than normal galaxies (Armus, Heckman, & Miley 1989, 1990). Based upon these results, the warm selection criterion is generally associated either with hidden AGN activity or with spatially concentrated star formation and is therefore useful in the study of the relationship between starburst and AGN activity in infrared galaxies by preferentially selecting objects with a large circumnuclear mass concentration.

We have chosen an *IRAS* color selection criterion which ensures that we have a sample containing many objects of mixed excitation class covering a wide range in FIR luminosity, but which will exclude most "normal" galaxies and ensure a high fraction of starburst, Seyfert, and LINER type galaxies. From the color-color diagrams of Dopita et al. (1998), we can see that Seyfert galaxies from Rush, Malkan, & Spinologlio (1993) generally lie below a F_{60}/F_{25} of 8. A selection criterion of $F_{60}/F_{25} < 8$ therefore selects optimally for Seyfert galaxies and warm starburst galaxies. We expect therefore that our results when compared with studies of samples which are not selected on IR color, will contain more AGN, direct or obscured. We based our sample selection upon the *IRAS* fluxes used by Strauss et al. (1992), which are from the *IRAS* Point Source Catalog, Version 2 (1988). We have now updated these fluxes to those in the *IRAS* Faint Source Catalog (Moshir et al. 1990, hereafter *IRAS* FSC). Fluxes presented in Table 1 are from the *IRAS* FSC.

Our sample is easily accessible from the south and is not appreciably affected by Galactic extinction. Table 1 lists positions, recessional velocity, distance in megaparsecs, derived FIR luminosity and IR luminosity, and *IRAS* FSC fluxes for the objects in our sample. Our sample was selected based on the FIR luminosity calculated following Sanders & Mirabel (1996) assuming an H_0 of 75 km s^{-1} Mpc^{-1} and q_0 of $\frac{1}{2}$:

$$L_{FIR} = 4\pi D_L^2 C F_{FIR}[L_\odot] , \quad (1)$$

where

$$F_{FIR} = 1.26 \times 10^{-14}\{2.58F_{60} + F_{100}\}[\mathrm{W\ m^{-2}}] . \quad (2)$$

The scale factor C is the correction factor required to account for the extrapolated flux for $F > 100$ μm, and D_L is the luminosity distance of the galaxy.

While our sample was selected using the FIR luminosity, we will use the infrared luminosity (L_{IR}) for the following analysis as it better represents the total mid- and far-infrared luminosity. This also enables easier comparisons with other samples, many of which have been selected on the basis of L_{IR}. The infrared luminosity was calculated following Sanders & Mirabel (1996) and is given by

$$L_{IR} = 4\pi D_L^2 F_{IR}[L_\odot] , \quad (3)$$

where

$$F_{IR} = 1.8 \times 10^{-14}\{13.48F_{12} + 5.16F_{25} + 2.58F_{60} + F_{100}\}[\mathrm{W\ m^{-2}}] . \quad (4)$$

The IR luminosity distribution for our sample is shown in

TABLE 1

SAMPLE PARAMETERS

This table is available only on-line as a machine-readable table

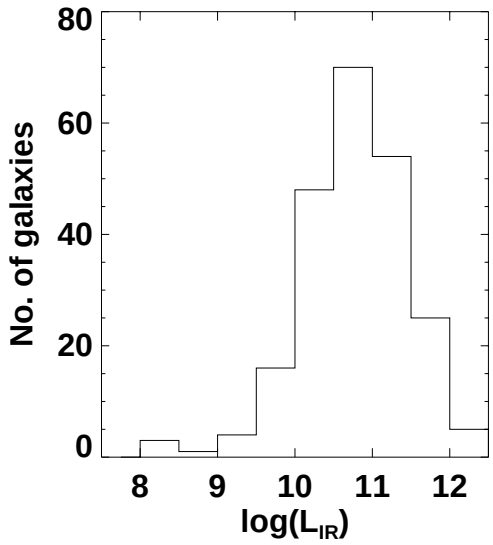

FIG. 1.—IR luminosity distribution for the 225 galaxies analyzed here. This distribution is identical to that of our entire sample of 285 galaxies.

Figure 1 and was calculated using the updated *IRAS* FSC fluxes.

3. OPTICAL SPECTROSCOPY

Our spectroscopic data were taken using the Double Beam Spectrograph (DBS) at the Mount Stromlo and Siding Springs 2.3 m telescope. This instrument is described in detail in Rogers, Conroy, & Bloxham (1988). We used 1200 lines mm^{-1} gratings in first order, giving a spectral resolution of 0.57 Å $pixel^{-1}$. We covered the ranges (6000–7000 Å) in the red and (4400–5400 Å) in the blue referred to the rest frame of the galaxies. The slit width was approximately 1″–2″ chosen to maximize the resolution with these gratings, giving 30 km s^{-1} at Hα and 50 km s^{-1} at Hβ. The spatial resolution was 1″ $pixel^{-1}$. Typically for galaxies having $cz = 8000$ km s^{-1} this corresponds to a spatial scale of ∼0.8 kpc, and for galaxies having $cz = 40{,}000$ km s^{-1}, to 4 kpc (assuming $H_0 = 75$ km s^{-1} Mpc^{-1} and $q_0 = 0.25$). Observations were acquired from 1996 January to 1997 June and are described in Table 2. Three exposures of 600 s were taken of each object, except where the object was faint, in which case four exposures were taken.

Data reduction was carried out using the IRAF package. This involved bias subtraction, flat-fielding, sky subtraction, wavelength calibration, atmospheric absorption correction, and flux calibration. Galaxy spectra were extracted using an aperture width corresponding to 1 kpc at the redshift of each galaxy. Wavelength calibration was derived using an Ne-Ar arc lamp spectrum taken during the same observing run and with rotator angle within 22°.5 of that for each object. This condition allows us to correct for minor wavelength shifts of the arc lines with rotator angle caused by flexure of the spectrograph structure. Second- or third-order polynomials in wavelength were fitted to typically 10 lines for each wavelength range giving rms residuals of ∼0.05–0.1 Å. The galaxies were corrected for atmospheric absorption by dividing the spectrum by a smooth spectrum standard star observed at the same air mass as the object. Flux calibration was performed using photometric standard star observations and is accurate to 20% for those galaxies observed under photometric conditions. However, as we are measuring line ratios, the error in absolute flux calibration is not of great concern. The optical spectra with a usable S/N ratio are presented in Figure 2.

TABLE 2

LOG OF OBSERVATIONS

This table is available only on-line as a machine-readable table

4. OPTICAL CLASSIFICATION

4.1. *Spectral Decomposition*

The spectral decomposition and extinction correction of our data has been described in detail in a previous paper (Kewley et al. 2000). We summarize these procedures briefly below.

The optical spectral line profiles were decomposed into multiple Gaussian components. While clearly the line emission in some galaxies is not necessarily Gaussian in shape, the principle aim here is to measure the flux in the various components of the line profile. For the purposes of standard line diagnostic analysis, the detailed shape of the fitted lines is unimportant provided the same profile is used for all emission arising from the same dynamical component.

The continua underlying the emission lines were subtracted using the "splot" task in IRAF. Where Hβ was contaminated by stellar absorption, the absorption was subtracted from the base of the observed Hβ emission line using splot and a Gaussian fit using the "ngaussfits" task in IRAF. We compared this method of fitting the underlying stellar absorption with the simultaneous fitting of two Gaussians, corresponding to the Hβ absorption and emission lines for IRAS 11149+0449, a galaxy in our sample containing a large Hβ absorption line and lower than average S/N ratio. We find that the Hβ emission line fluxes derived from these two methods differ by 3%, which corresponds to 0.02 dex on the diagnostic diagrams. We conclude that our resolution is sufficient that, at Hβ, the stellar absorption line is well resolved and easily distinguished from the nebular emission line, and is such that the local continuum fitting gives the true intensity of the emission line to within a few percent.

The line profiles were decomposed into Gaussians using ngaussfits in IRAF. This routine uses least squares fitting implemented by a downhill simplex minimization algorithm. Our Gaussian decomposition proceeds on the assumption that narrow lines are produced in the same region within each galaxy.

The wavelength and flux of [N II] λ6548 was fixed to that of [N II] λ6584 using the observational value $\lambda([\mathrm{N\ II}]\ \lambda6548/\lambda([\mathrm{N\ II}]\ \lambda6584) = 0.9946$ and the theoretical [N II] flux ratio $F(\lambda6548)/F(\lambda6583) = 0.3396$. We can measure the flux in the emission lines down to 1 σ, where σ is the noise in the spectrum at the wavelength of the emission line integrated over the full width of the emission line profile. We have optical spectra containing emission line data to be able to plot points on either or both of the [N II] λ6584/Hα versus [O III] λ5007/Hβ and [S II] λλ6717, 31/Hα versus [O III] λ5007/Hβ diagnostic diagrams for a total of 225 galaxies.

For some galaxies, broad components of Hα and Hβ were required to produce a satisfactory fit to the line profile.

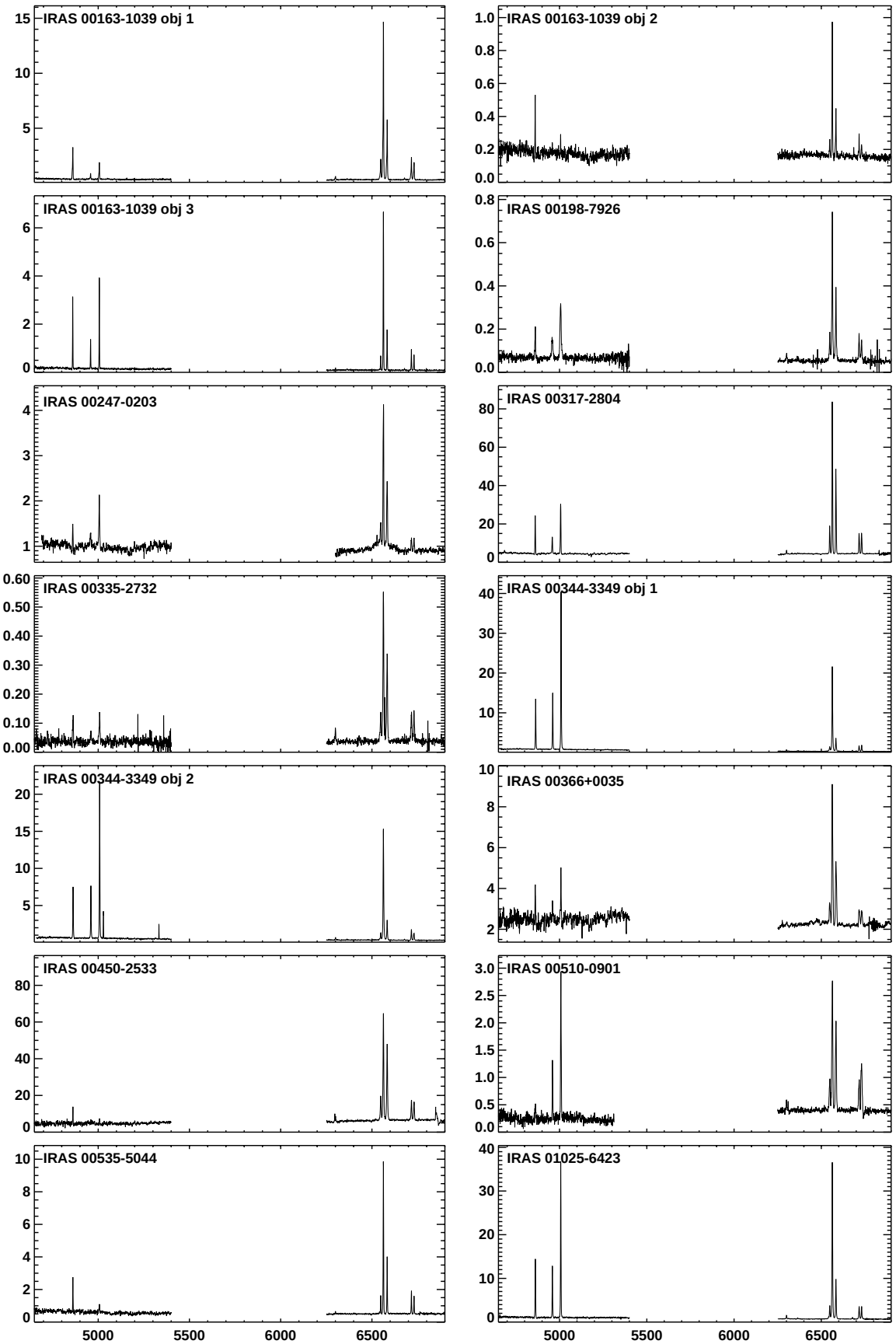

FIG. 2.—Optical spectra for the galaxies in our sample. Spectra have been converted to zero redshift. Flux is in units of 1×10^{-15} ergs s^{-1} cm^{-2} $Å^{-1}$.

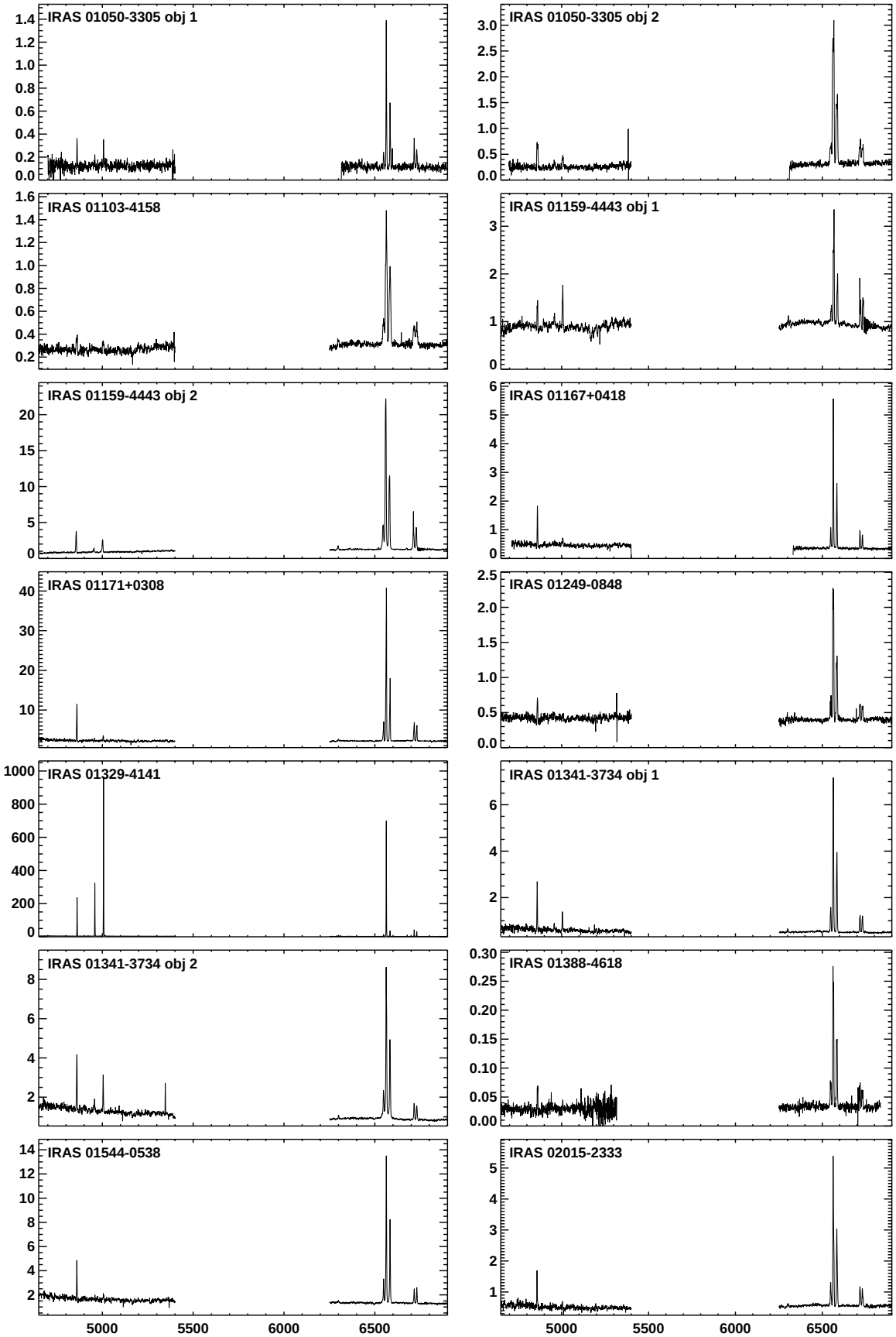

FIG. 2.—*Continued*

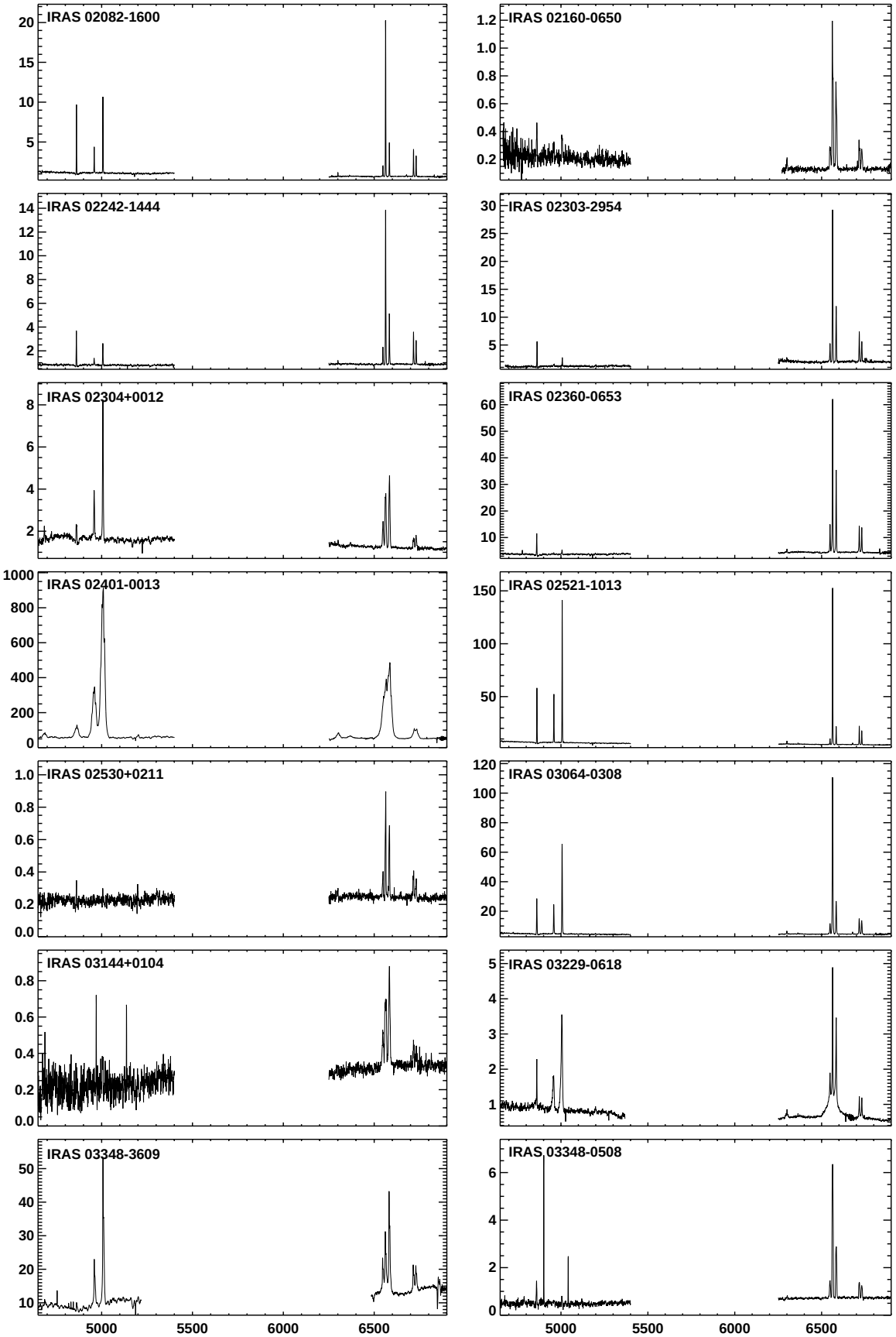

FIG. 2.—*Continued*

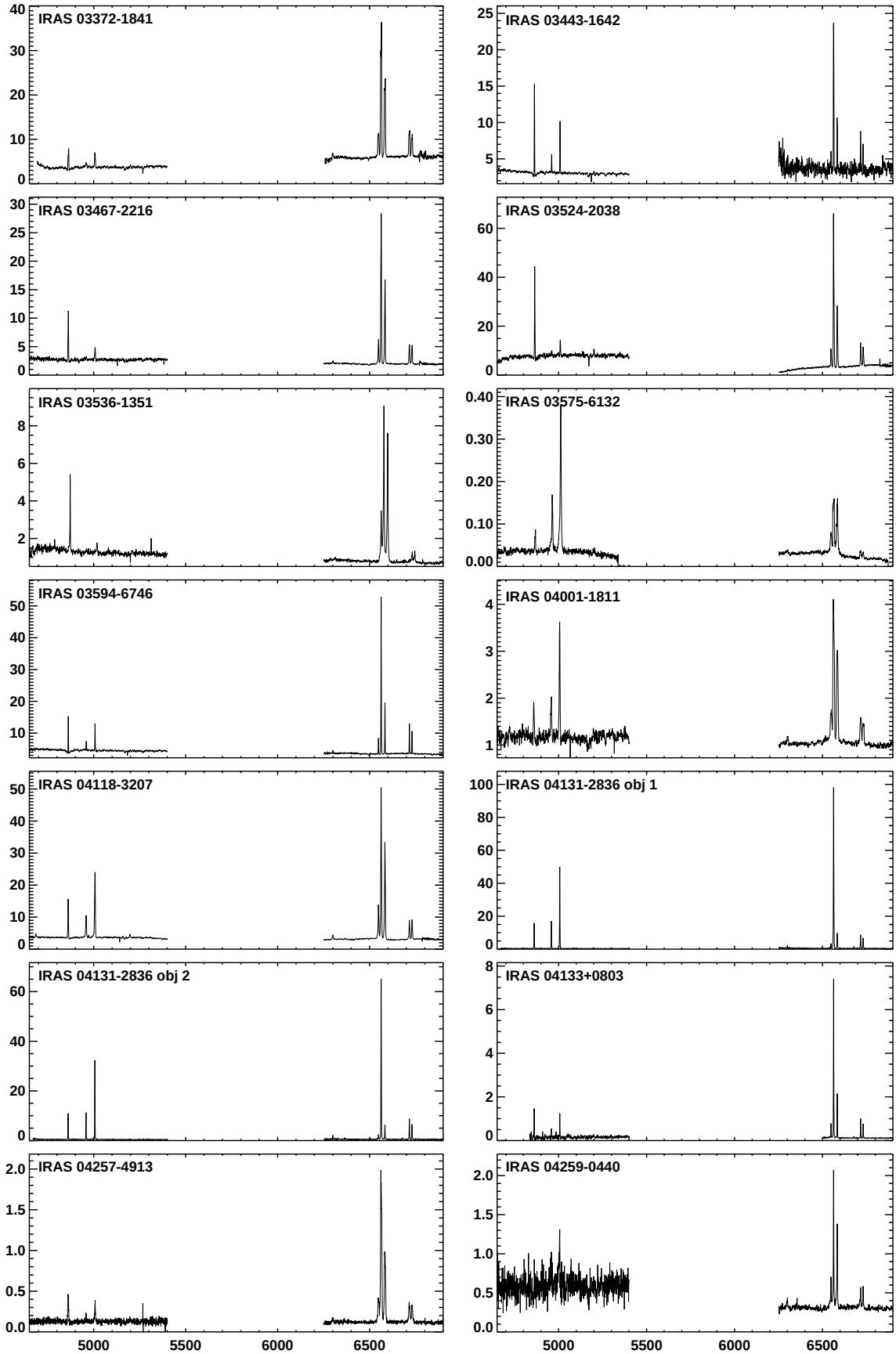

FIG. 2.—*Continued*

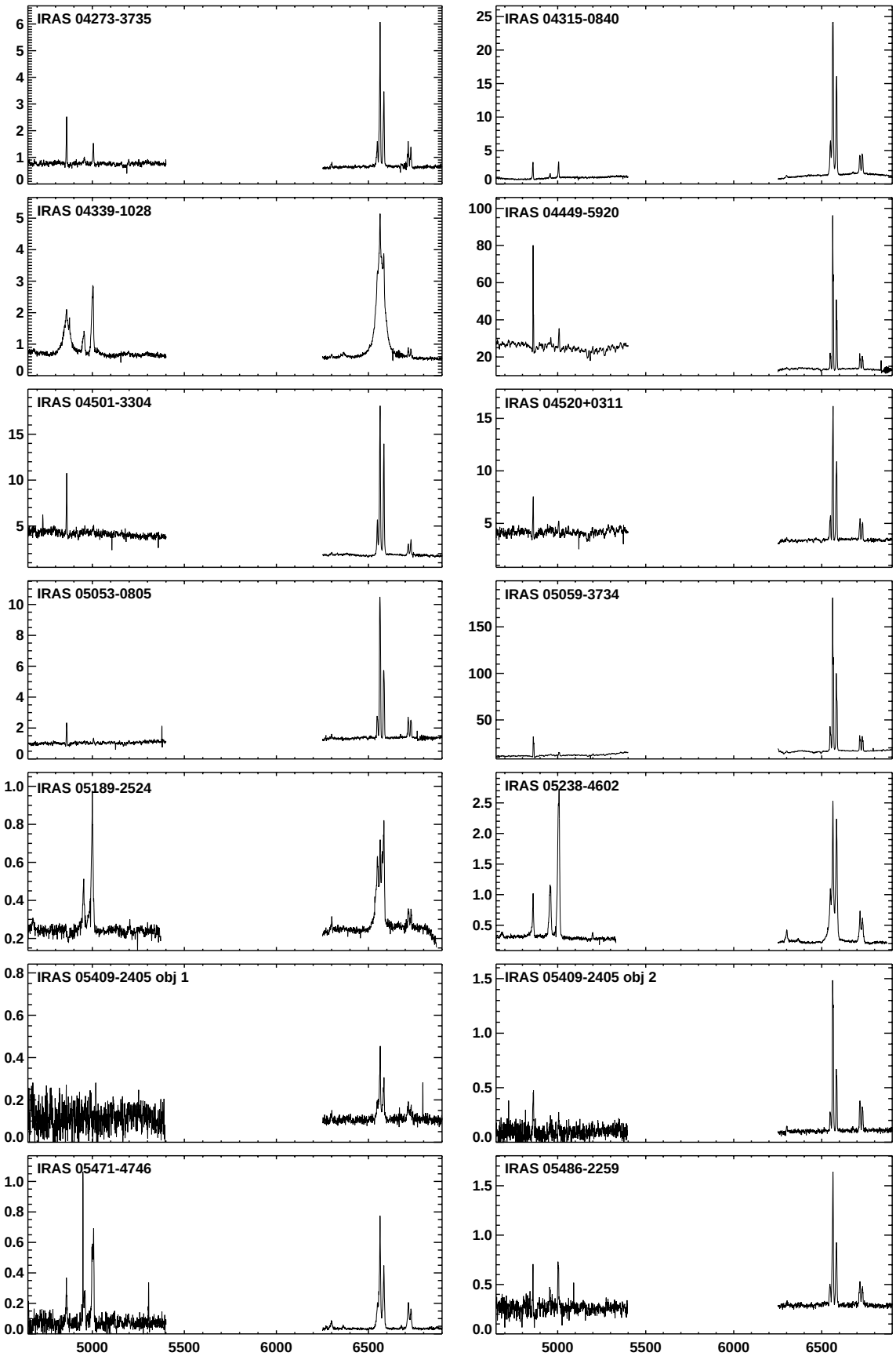

FIG. 2.—*Continued*

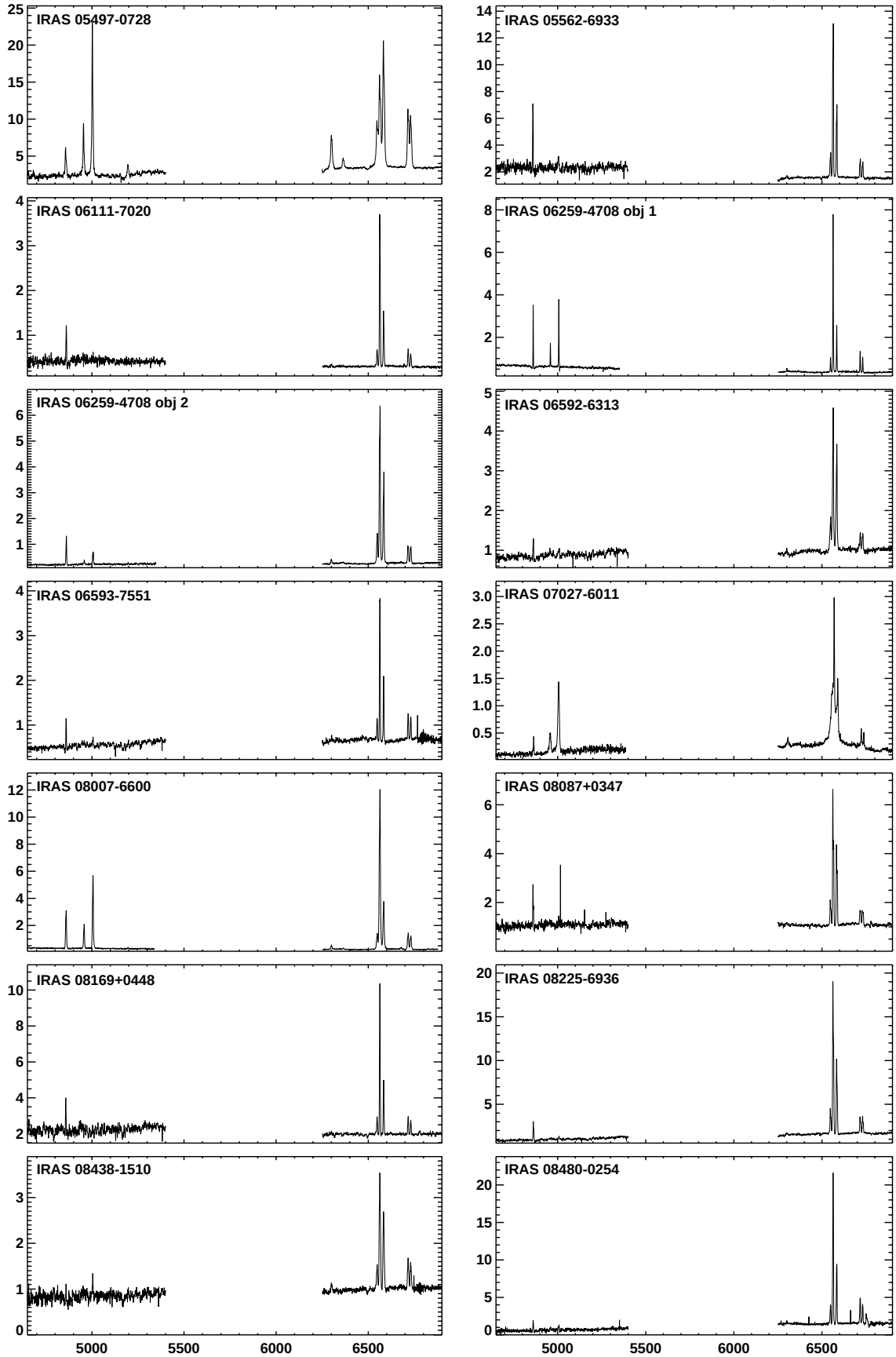

FIG. 2.—*Continued*

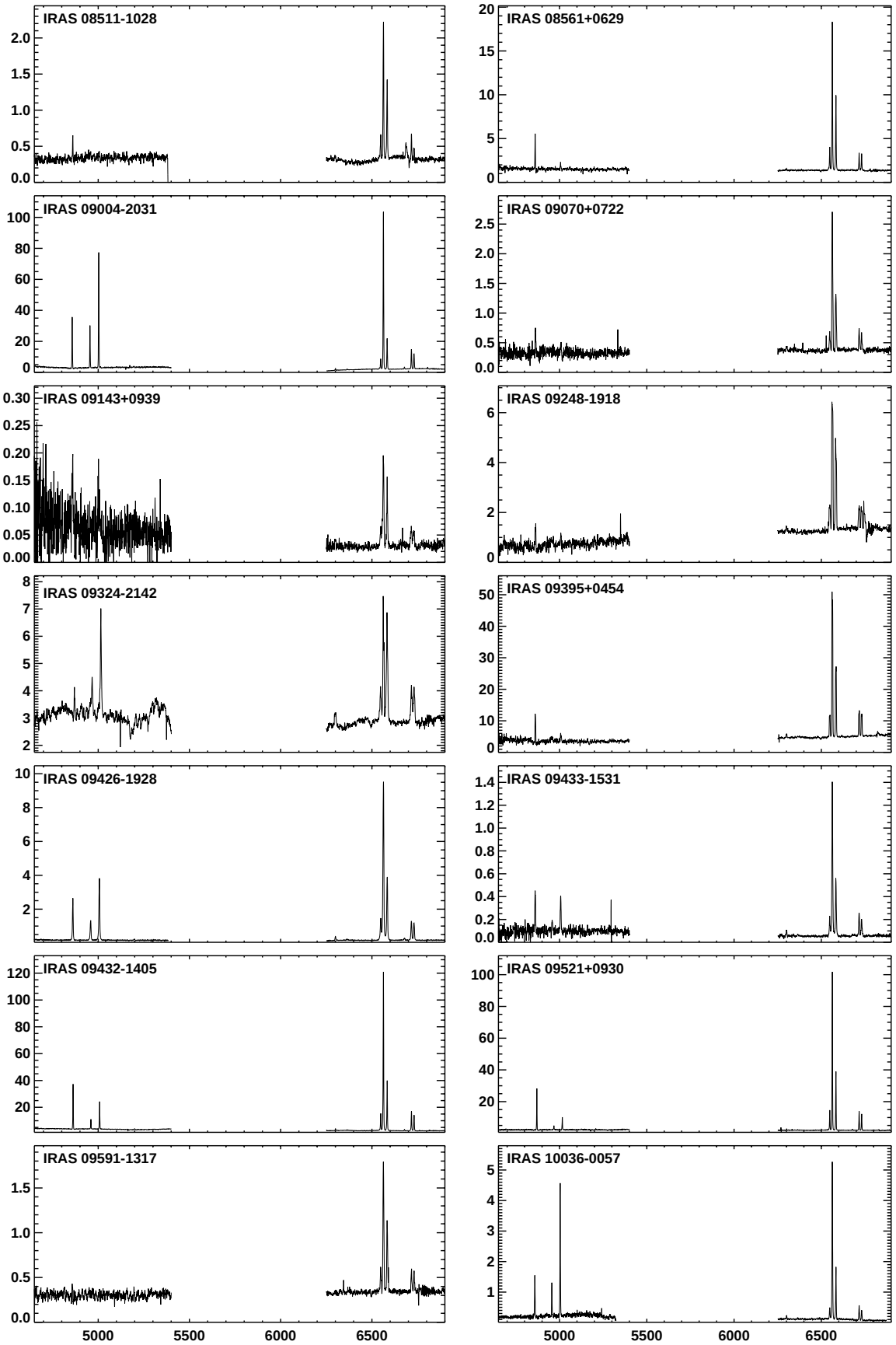

FIG. 2.—*Continued*

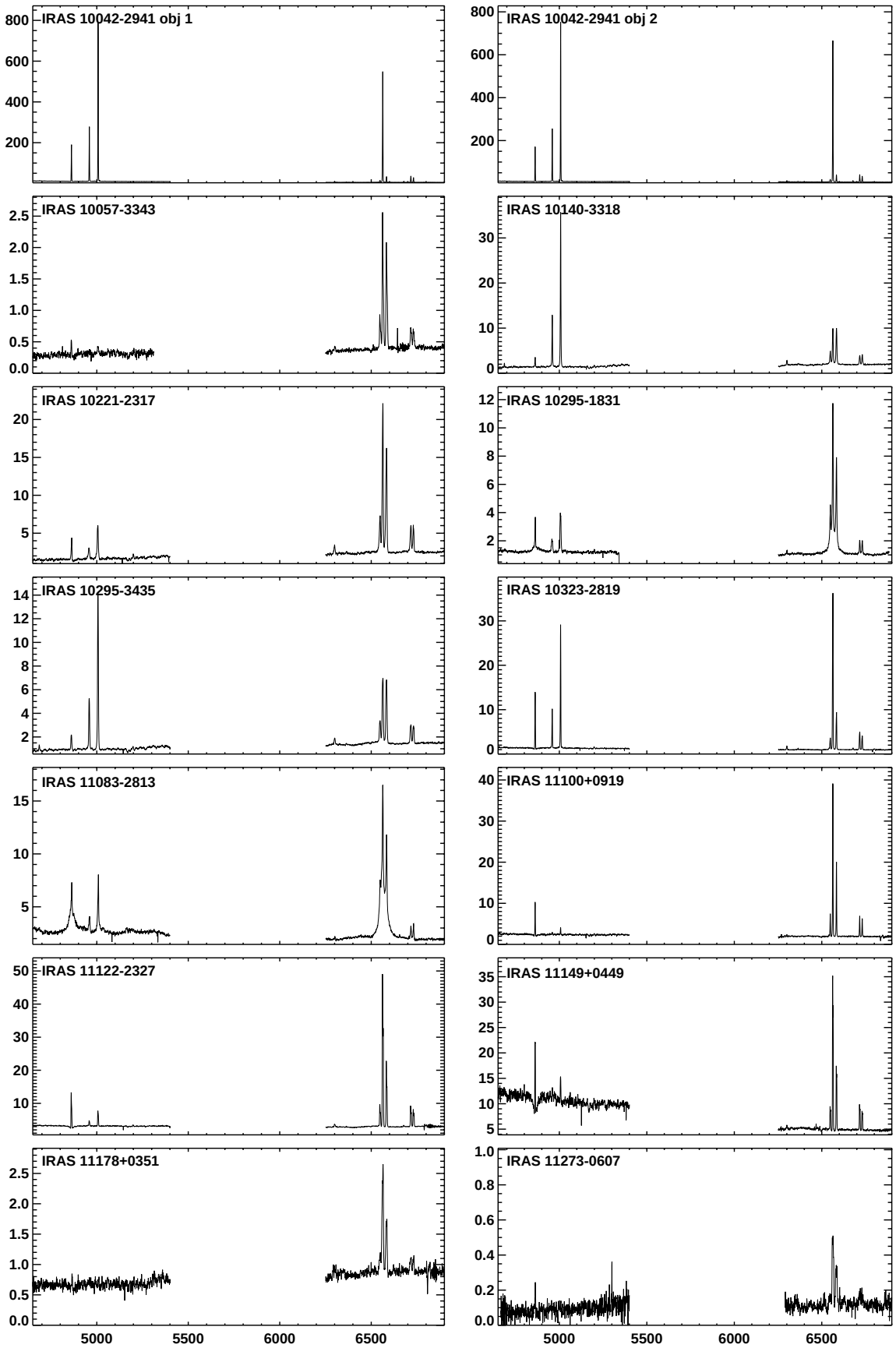

FIG. 2.—*Continued*

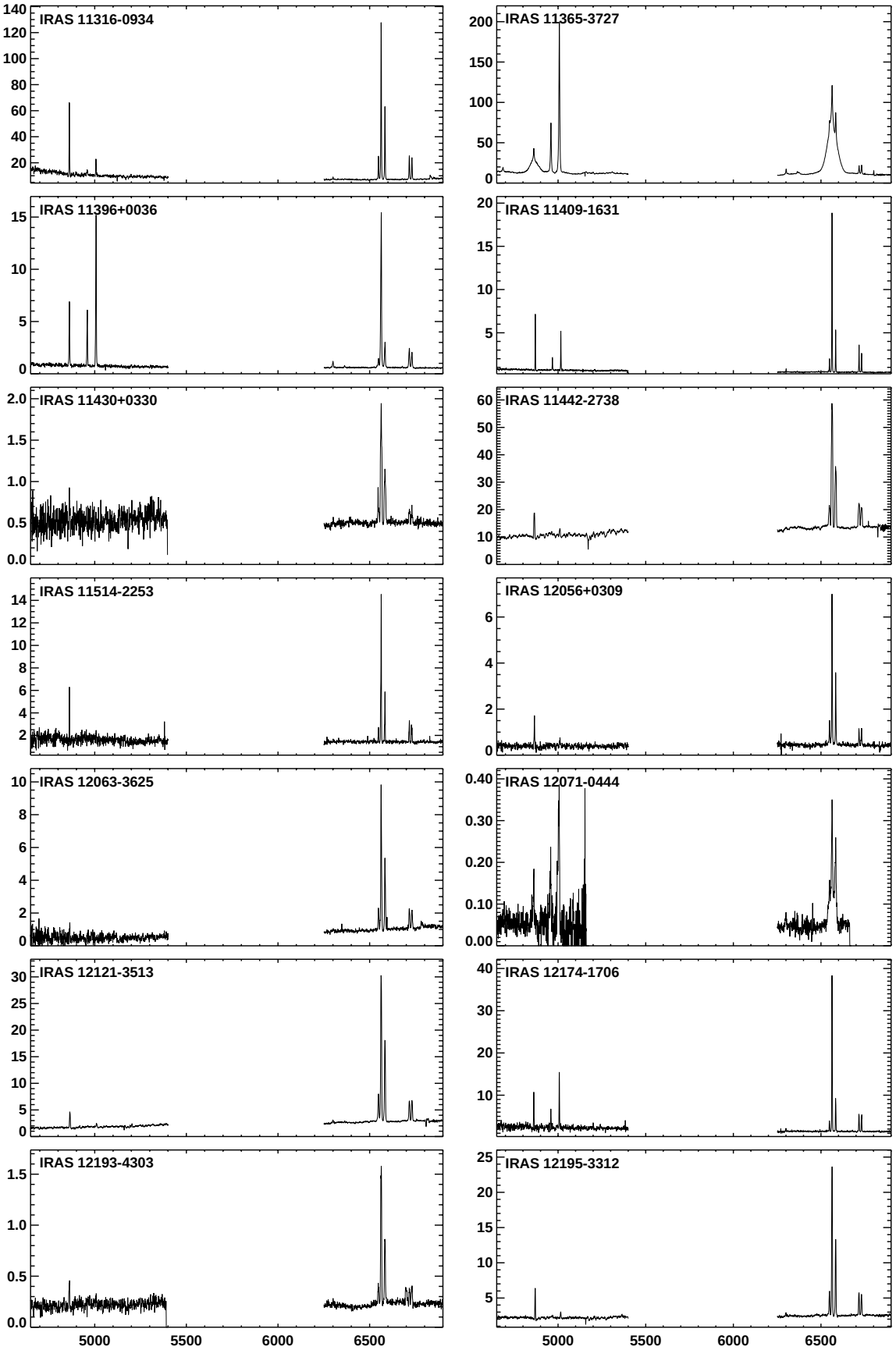

FIG. 2.—*Continued*

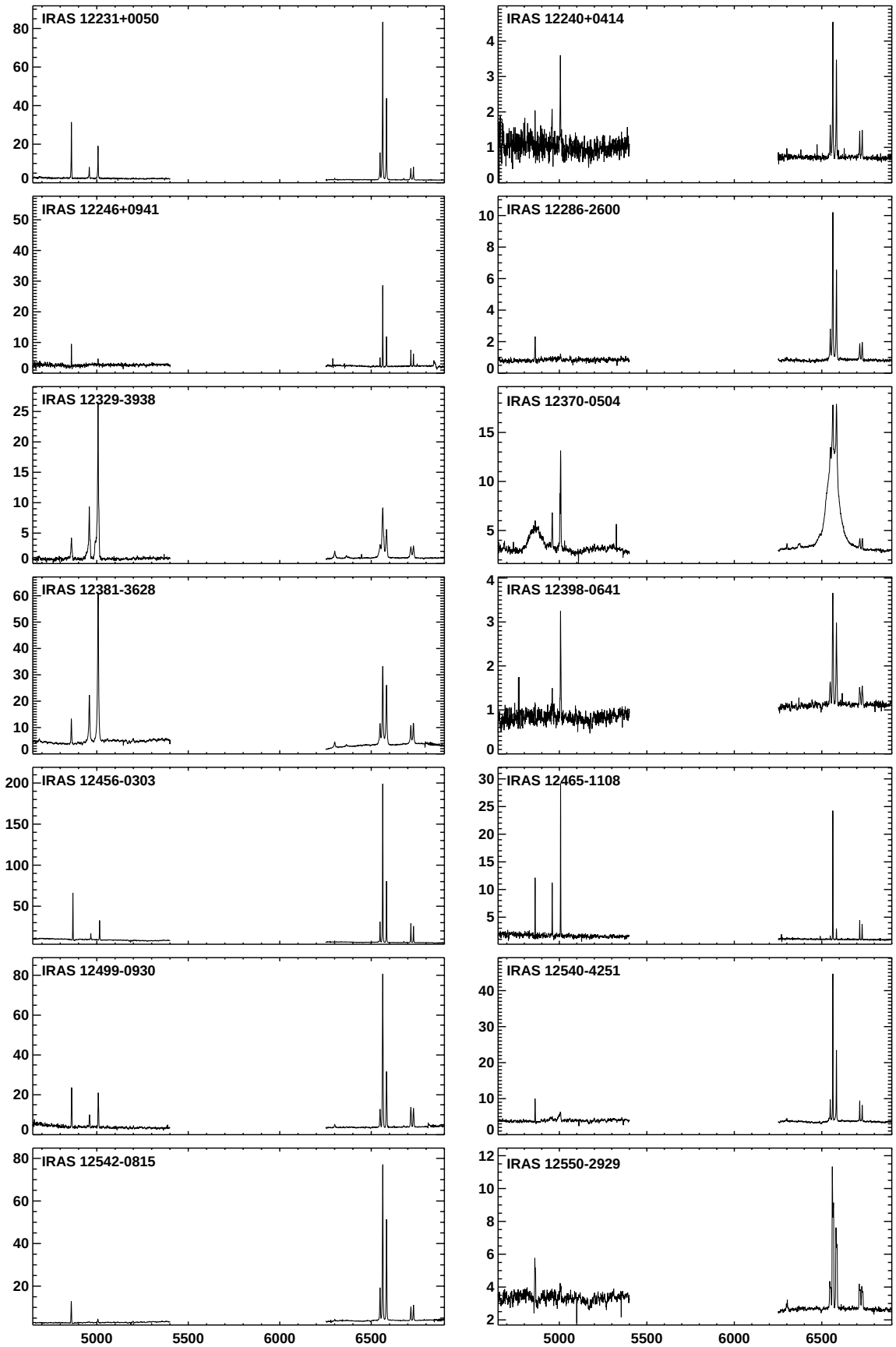

FIG. 2.—*Continued*

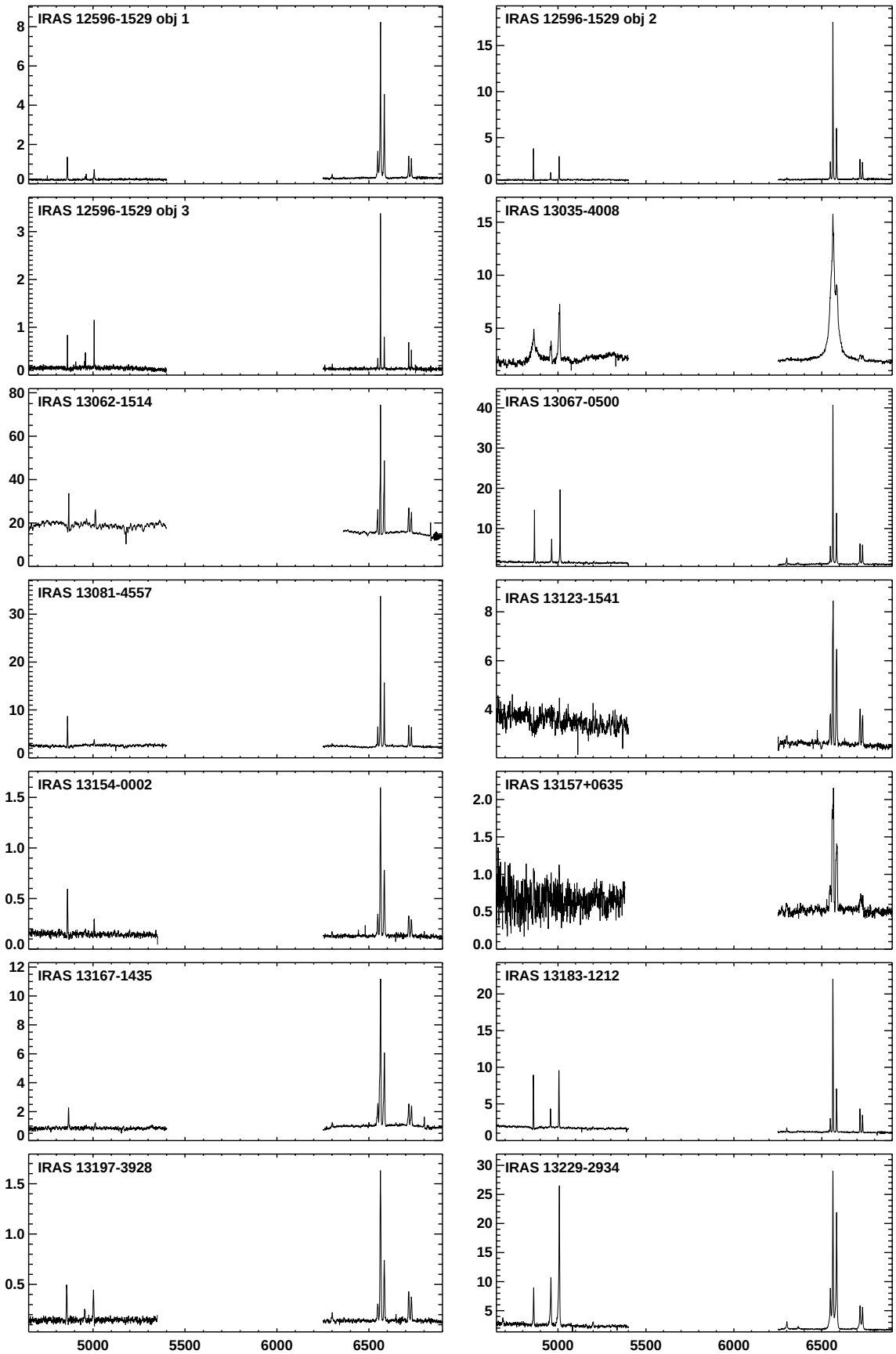

FIG. 2.—*Continued*

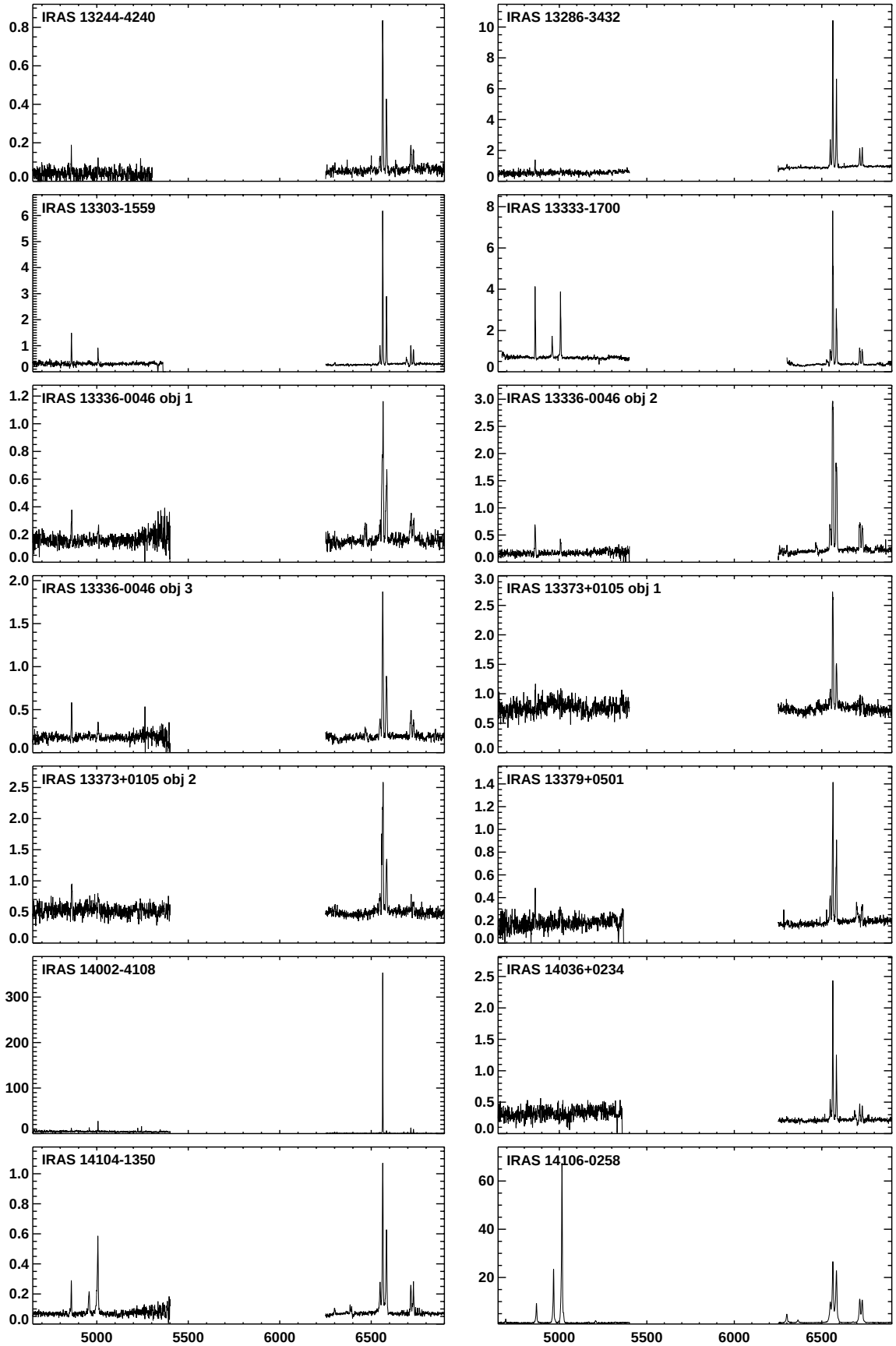

FIG. 2.—*Continued*

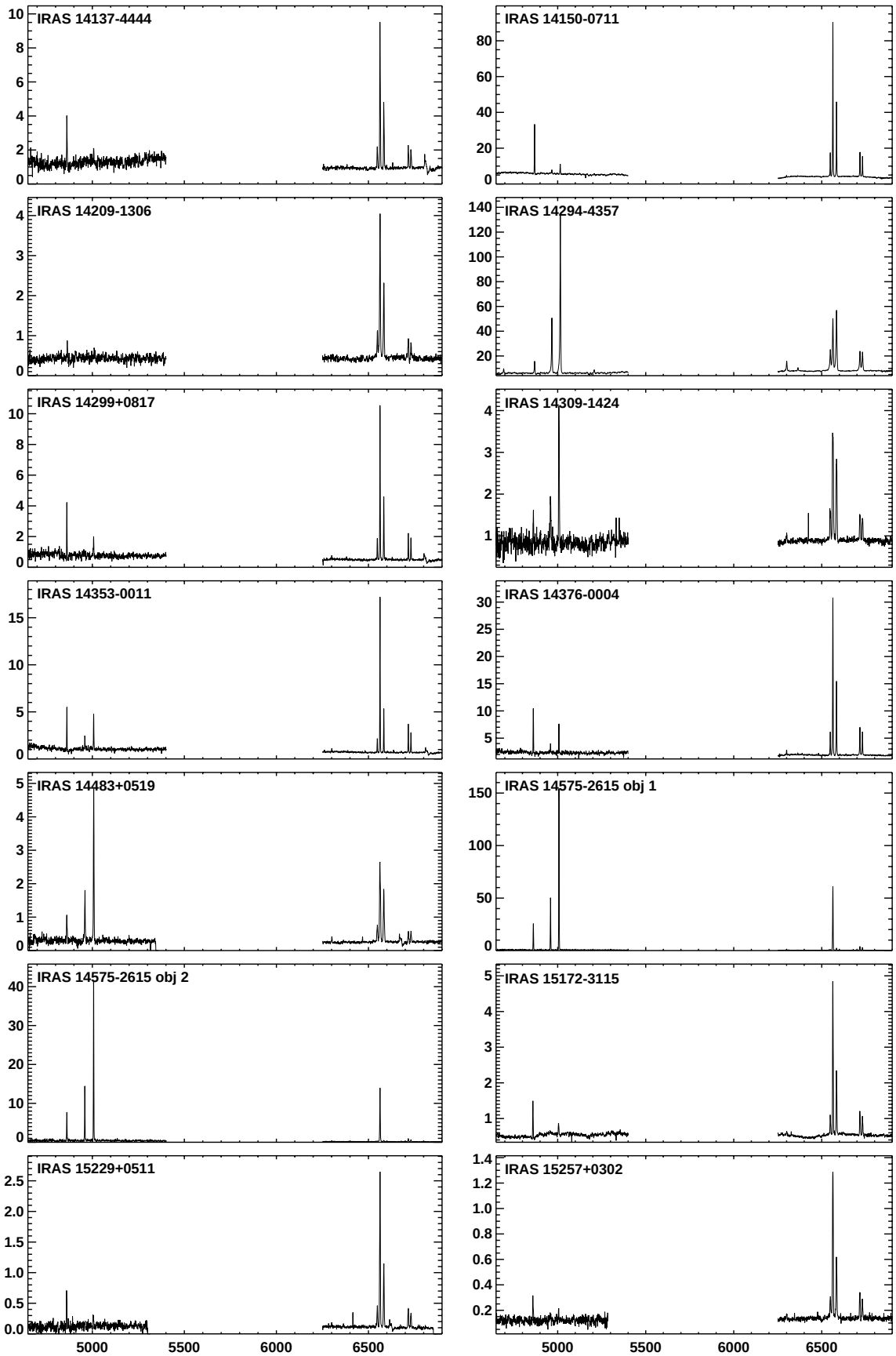

FIG. 2.—*Continued*

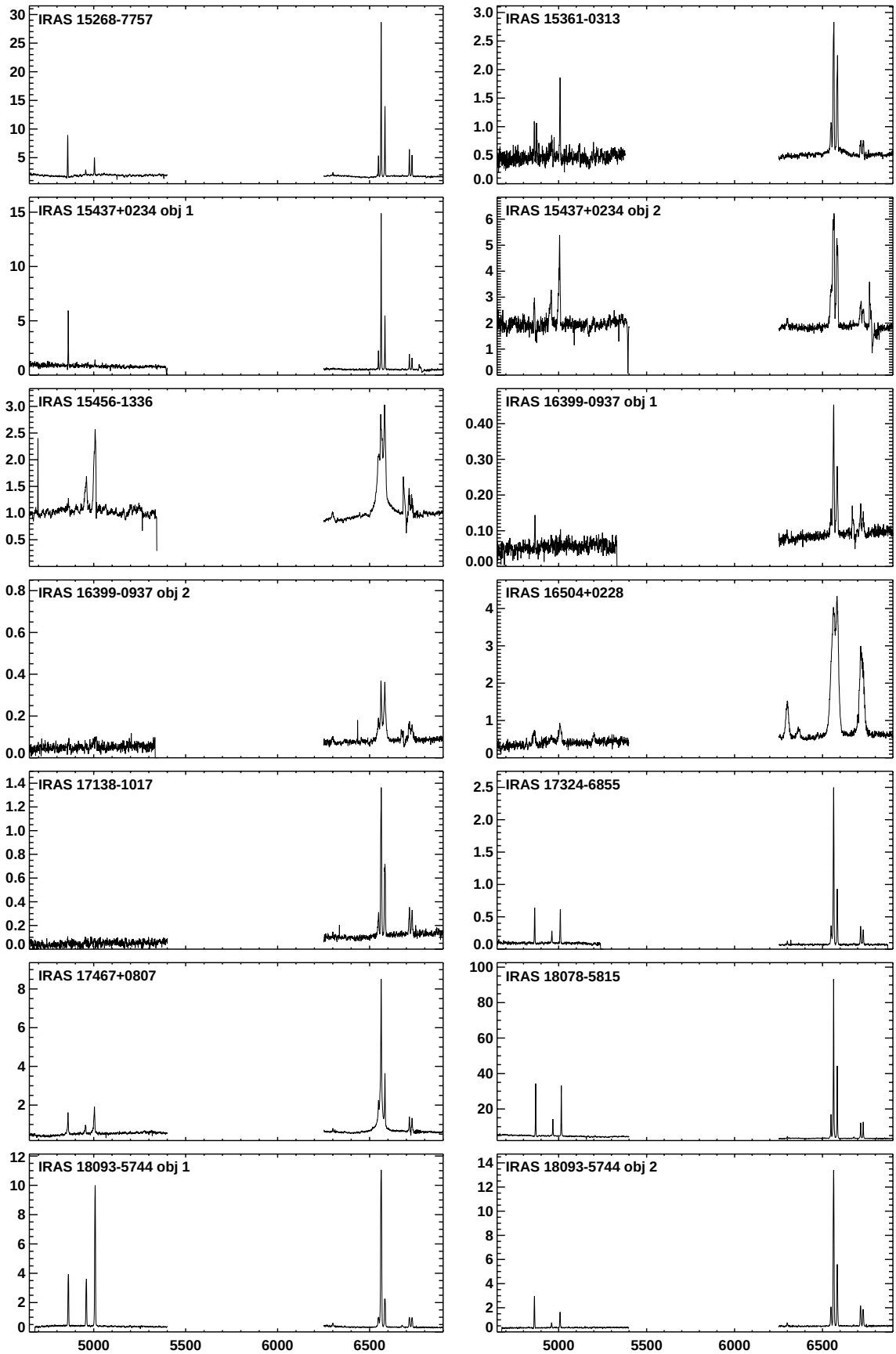

FIG. 2.—*Continued*

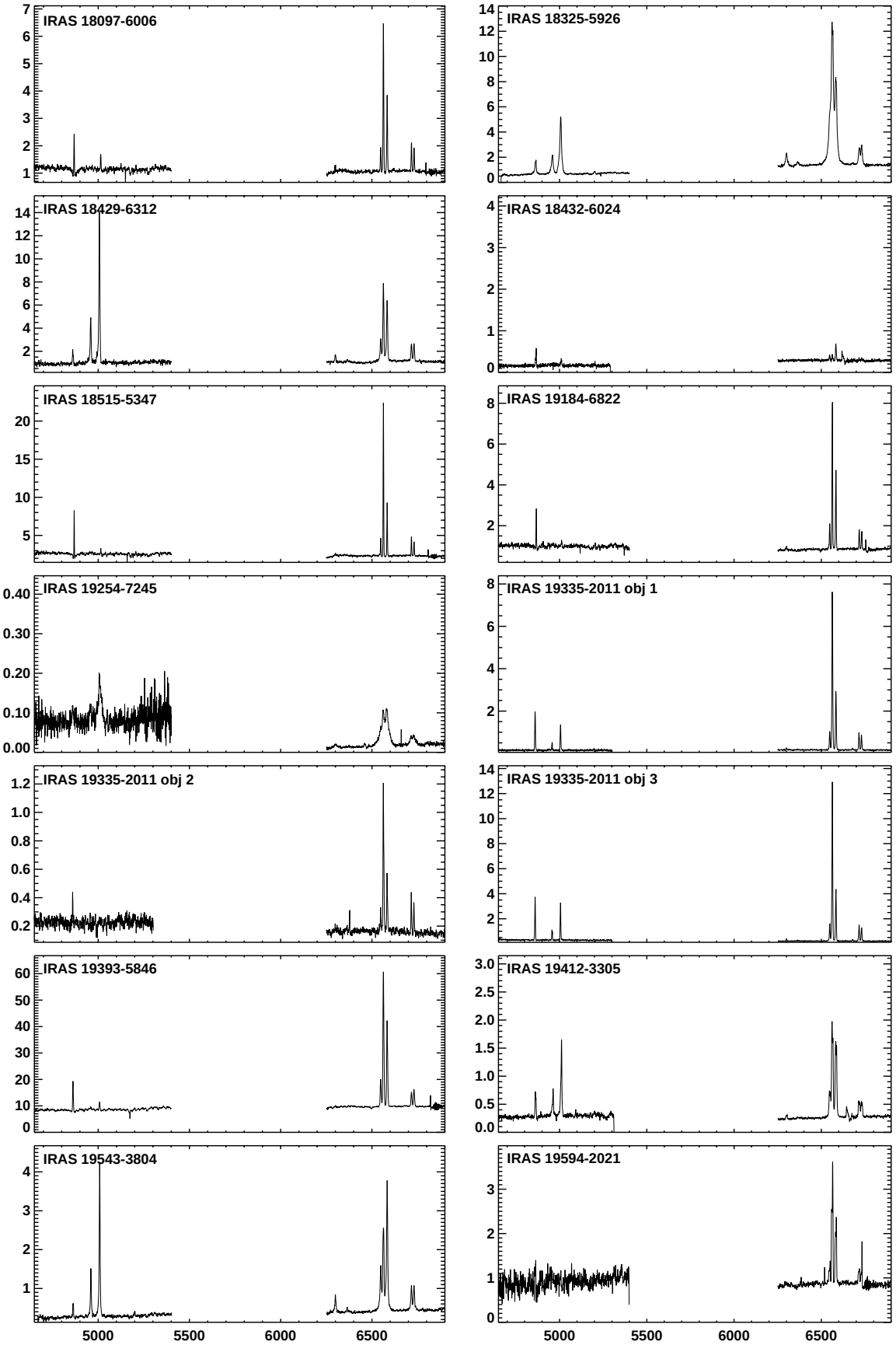

FIG. 2.—*Continued*

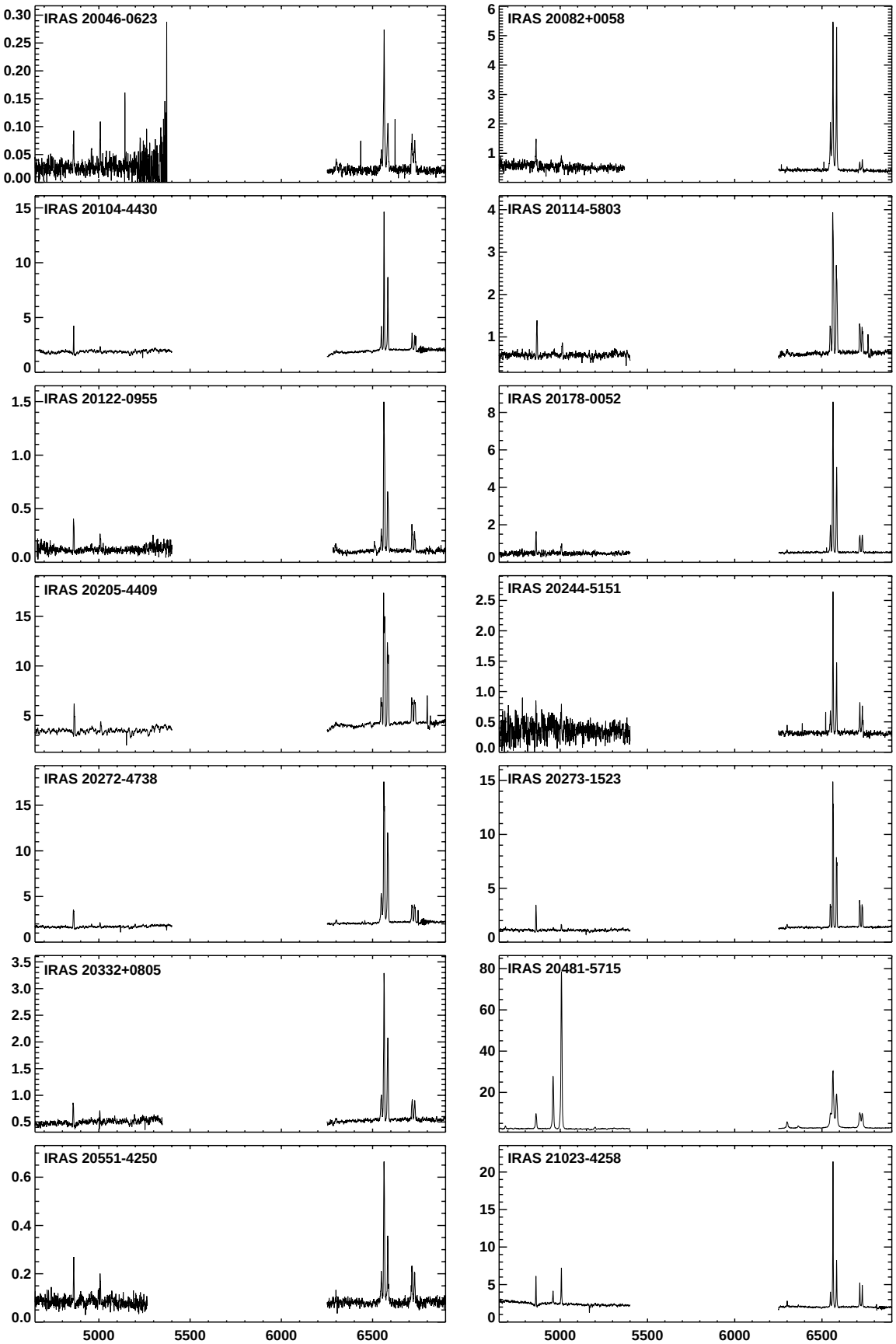

FIG. 2.—*Continued*

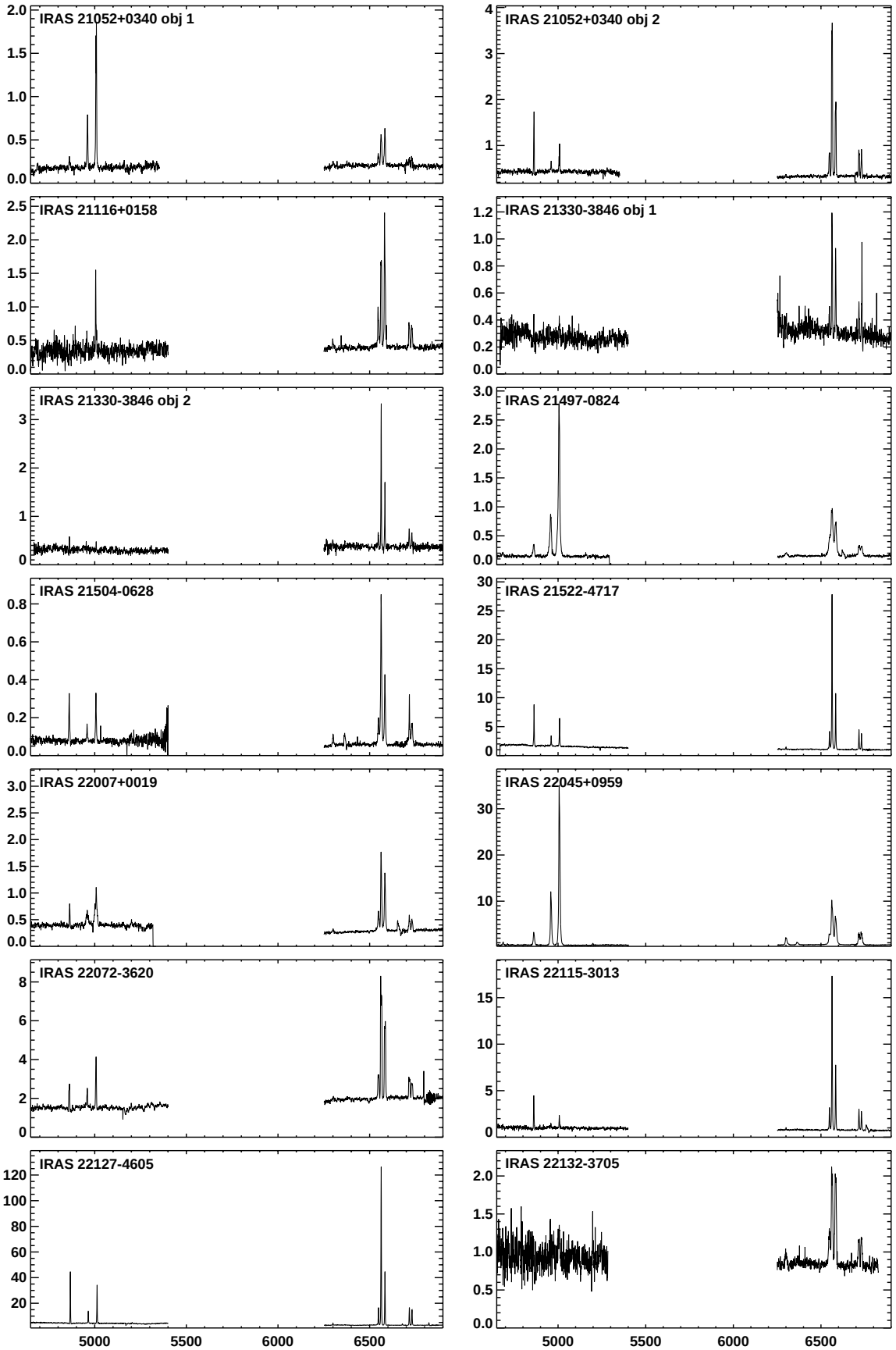

FIG. 2.—*Continued*

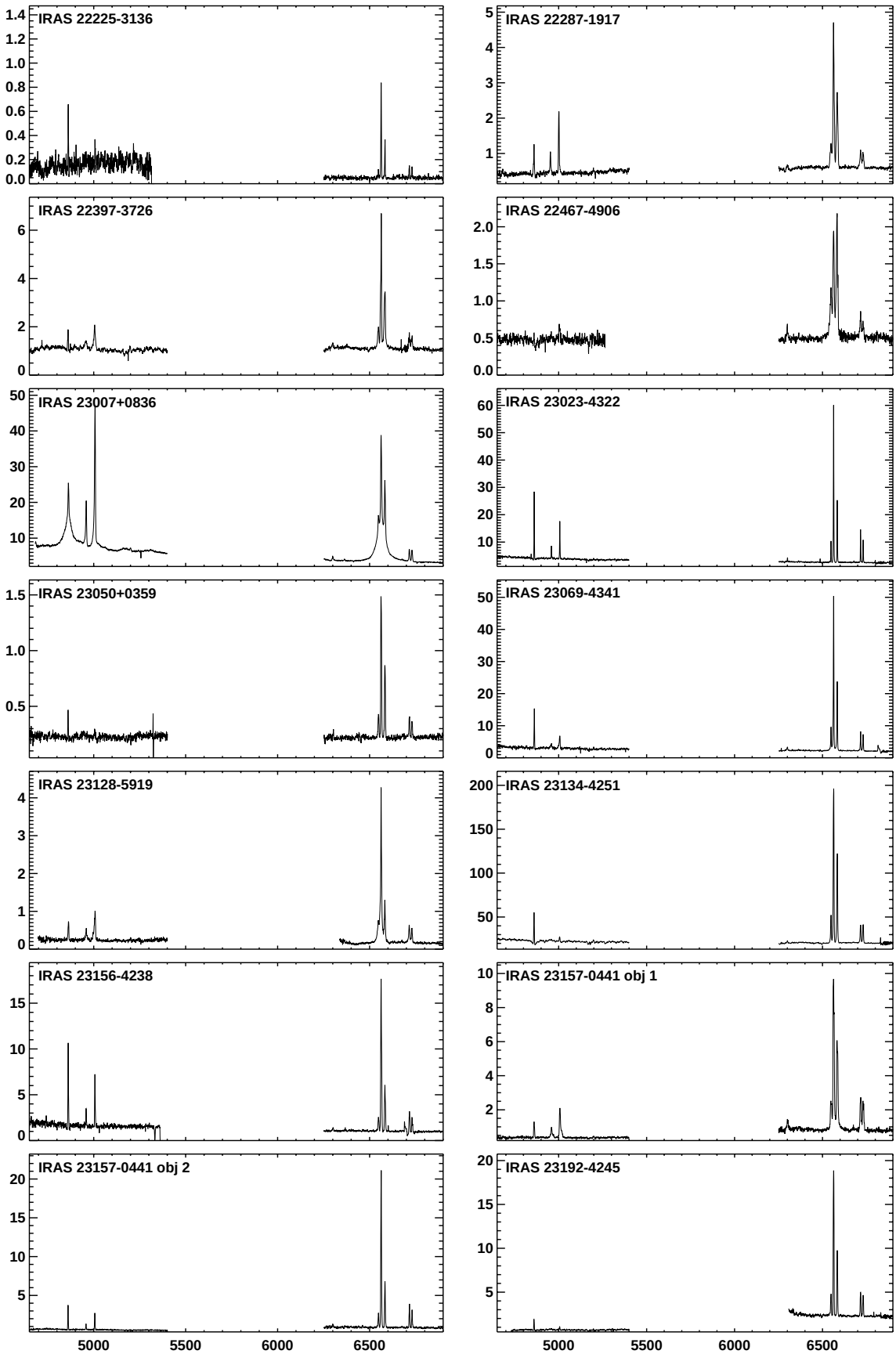

FIG. 2.—*Continued*

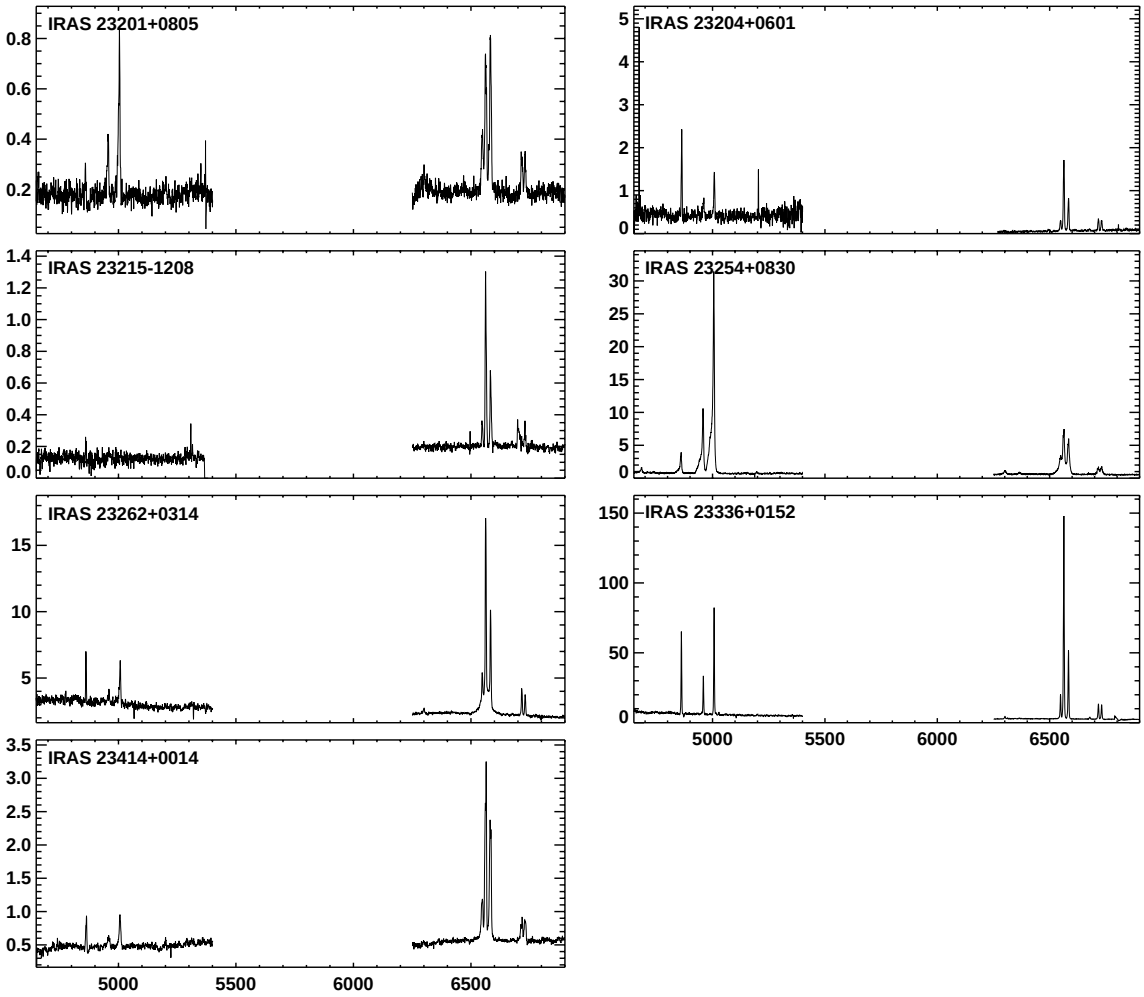

FIG. 2.—*Continued*

If the rms deviation of the Chi-square of the fit to the observational line profile was at least 25% less with a broad component added, then a broad Hα was included in the spectral decomposition.

In Table 3, we present the measured flux ratios for the narrow-line components of the galaxies.

Some 17 galaxies in our sample display asymmetries in the line profiles. Asymmetries in the [O III] λ5007 line have been extensively studied by Whittle (1985) and Heckman et al. (1981). The majority (16/17) of the asymmetries in our sample are blueshifted and probably result from outflows of gas with distributed opaque clouds. It is also possible that inflow of gas with opaque clouds internal to the narrow-line emitting region could produce the blue asymmetry. Studies of H I absorption and the velocity field of the absorbing region have found that both inflows and outflows occur in narrow-line emission galaxies (see, e.g., Mirabel 1982 and Heckman et al. 1981). Alternatively, the asymmetries may arise from separate regions of line emitting gas, with different gas velocities. The asymmetric profiles in the galaxies in our sample can be fitted very well by two Gaussians, one for the narrow component described above, and the other being a broader component shifted to the blue. The flux within this blue broad component has no meaning itself, but the combined flux of both the narrow and blueshifted Gaussians is a much more reliable method for measuring the line ratios than by using the flux in the narrow component alone. These galaxies are marked by a "1" in Table 3 and are described in further detail in § 5.6 and in the Appendix.

Some eight AGN-type galaxies have [O III] lines which are up to 4 times broader than the remaining narrow emission lines. This is most likely due to the [O III] emitting region being closer to the AGN nucleus. It therefore has higher gas velocity and velocity dispersion than the regions emitting the remainder of the optical lines. Due to differences in line profile shape, for some cases, a single broader Gaussian was fitted to the [O III] lines and for some cases narrow plus broader components were used. All objects with broad [O III] lines are described in the Appendix.

One galaxy, IRAS 05189−2524 has a very complex line profile. It either has two narrow components to each narrow emission line and a broad Hα, or three components to each narrow emission line comprising two narrow components and a blueshifted broader component. The rms deviation of the Chi-square of the fit is very similar for both

TABLE 3

MEASURED FLUX RATIOS

This table is available only on-line as a machine-readable table

models, and it is unclear which of these models is correct. Young et al. (1996) fitted two narrow components to each narrow emission line and a broad Hα to the red spectrophotometric profile of this galaxy, classing it as a Seyfert 2. The Hβ line is only seen in absorption in this galaxy, indicating an old stellar population. The strength of the [N II] λ6584, [S II] λλ6717,31 lines indicate Seyfert activity.

The flux in the [S II] λλ6717,31 forbidden lines in our spectra were used in conjunction with a five-level model atom using our MAPPINGs code (Sutherland & Dopita 1993) to estimate the (emission measure weighted) mean electron density within the 1 kpc region extracted for our galaxies. The [S II] λλ6717,31 flux ratios and electron densities calculated can be found in Table 3.

4.2. *Extinction Correction*

The emission-line spectra were corrected for reddening following VO87. We used the Whitford reddening curve as parameterized by Miller & Mathews (1972). The intrinsic flux ratio of H II region–like objects was assumed to be $I(\mathrm{H}\alpha)/I(\mathrm{H}\beta) = 2.85$, and for the AGN-like objects, we have assumed $I(\mathrm{H}\alpha)/I(\mathrm{H}\beta) = 3.1$

The flux values of the Gaussian decomposition of the forbidden lines in Table 3 have been corrected for reddening, except for the flux given for the Hα/Hβ ratio. The extinction coefficient $E(B-V)$ calculated is shown for each galaxy.

4.3. *Diagnostic Diagrams*

The VO87 diagnostic diagrams provide an excellent means of classifying galaxies by easily measured line ratios alone. They consist of the log ([O III] λ5007/Hβ) line ratio on the y-axis against log ([N II] λ6584/Hα), log ([S II] λλ6717,31/Hα), or log ([O I] λ6300/Hα) on the x-axis. Starbursts fall onto the lower left-hand region of these plots, narrow-line Seyferts are located in the upper right and LINERs are in the lower right-hand zone. We present these diagrams in Figure 3 for the galaxies in our sample. What is striking about the distribution of points is their fairly tight grouping, indicating a surprising degree of homogeneity in the sample. VO87 derived a semiempirical boundary line used to separate starbursts from Seyferts with these diagrams. Here we present for the first time theoretical boundary lines which may be used to classify starbursts, Seyferts and LINERs.

4.3.1. *Starburst Modeling*

In order to place a theoretical upper limit on starburst activity on the optical diagnostic diagrams, we have carried out detailed continuous starburst modeling using the stellar population synthesis model PEGASE 2.0 (Fioc & Rocca-Volmerange 1997) combined with our MAPPINGs v3.0 photoionization and shock code (Sutherland & Dopita 1993). The photoionization models used here are identical to the PEGASE + MAPPINGs v3.0 continuous models described in Dopita et al. (2000) except that we have used an electron density of 350 cm^{-3}, which is the average electron density for the galaxies in our sample. We describe the models briefly here and refer the reader to Dopita et al. (2000) for further details.

The PEGASE 2.0 code uses the Kurucz (1992) plane-parallel LTE model atmospheres for stars with effective temperatures $T_{\mathrm{eff}} < 50{,}000$ K and the models of Clegg & Middlemass (1987) for hotter stars. The stellar atmospheres formulation is that of Lejeune, Cuisinier, & Buser (1997), covering the entire Hertzsprung-Russell diagram (HRD). We have assumed the initial mass function (IMF) to be of the Salpeter form ($\alpha = 2.35$), with a lower mass cutoff of 0.1 $M_\odot$ and an upper mass cutoff of 120 $M_\odot$. The actual value of the lower mass cutoff is unimportant, since only stars of mass greater than 15 $M_\odot$ contribute to the ionizing continuum. The upper mass cutoff could be taken to be anywhere between 80 and 120 $M_\odot$. However, Stasińska & Leitherer (1996) showed that EUV spectrum is insensitive to this parameter, provided it is not set too low.

We have compared the PEGASE code with another stellar population synthesis code, STARBURST99 (Leitherer et al. 1999). We find that PEGASE produces ionizing stellar continua which when combined with our MAPPINGs code and a realistic range of ionization parameter and metallicity, reproduces the observed line ratios for our warm infrared galaxy sample very well. An analysis of the differences between the models and the effects of the stellar tracks used are the subject of a future paper.

We used the PEGASE models to produce the ionizing stellar continuum for our photoionization and shock modeling using MAPPINGs. We found that, with a realistic range of metallicities ($Z = 0.1$–3.0) and ionization parameter q (cm s^{-1}) in the range $5 \times 10^6 \leq q \leq 3 \times 10^8$ (or $-3.5 \leq \log \mathscr{U} \leq -2.0$), continuous starburst models always fall below and to the left of an empirical limit on the [N II] λ6584/Hα versus [O III] λ5007/Hβ, [S II] λλ6717,31/Hα versus [O III] λ5007/Hβ, and [O I] λ6300/Hα versus [O III] λ5007/Hβ diagrams. This is due to the grid of the ionization parameters and metallicities folding over upon itself, shown in Dopita et al. (2000). Varying these parameters cannot change these maximum starburst lines. The lines representing these theoretical starburst limits are shown in Figure 3 and can be parameterized by the following simple fitting formulae:

$$\log\left(\frac{[\mathrm{O\ III}]\ \lambda 5007}{\mathrm{H}\beta}\right) = \frac{0.61}{\log\left([\mathrm{N\ II}]/\mathrm{H}\alpha\right) - 0.47} + 1.19\,, \tag{5}$$

$$\log\left(\frac{[\mathrm{O\ III}]\ \lambda 5007}{\mathrm{H}\beta}\right) = \frac{0.72}{\log\left([\mathrm{S\ II}]\ \lambda\lambda 6717{,}31/\mathrm{H}\alpha\right) - 0.32} + 1.30\,, \tag{6}$$

$$\log\left(\frac{[\mathrm{O\ III}]\ \lambda 5007}{\mathrm{H}\beta}\right) = \frac{0.73}{\log\left([\mathrm{O\ I}]\ \lambda 6300/\mathrm{H}\alpha\right) + 0.59} + 1.33\,. \tag{7}$$

The shape and position of this maximum starburst line has not been previously established from theoretical models, since the shape of the ionizing spectrum of the cluster was not known to sufficient accuracy. VO87 have attempted to establish both the position and the shape of this boundary in a semiempirical way, using both observational data from the literature and the models available to them at that time.

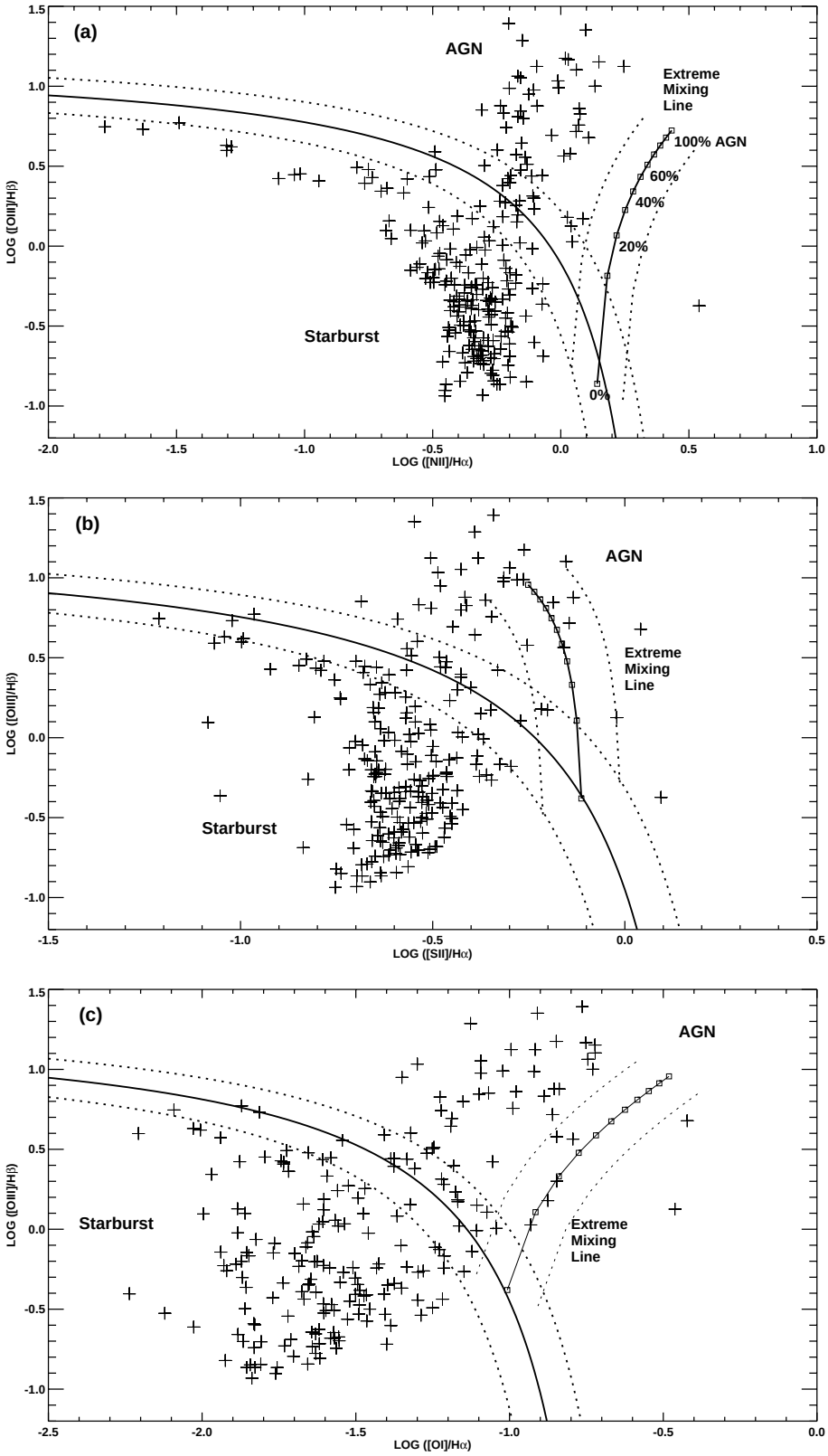

FIG. 3.—Diagnostic diagrams showing the galaxies in our sample. Our theoretical classification line and extreme mixing line are shown in bold; dashed lines represent ±0.1 dex of these lines, indicating the error range of our modeling.

The theoretical boundaries for starbursts defined by equations (5)–(7) provide us for the first time with a theoretical, as opposed to a semiempirical boundary for the region occupied by starbursts in these diagnostic plots. In view of the potential for errors in the modeling which may flow from errors in the assumptions made in the chemical abundances, chemical depletion factors, the slope of the initial mass function, or in the stellar atmosphere models, we have

included estimates of these errors as dashed lines in Figure 3.

4.3.2. *AGN Modeling*

The AGNs are modeled as 500 km s^{-1} radiative shocks with photoionized precursors (Dopita & Sutherland 1995) for metallicities $Z = 0.1$, 0.2, 0.5, 1.0, 1.5, 2.0, 3.0 solar and ionization parameter q between 5×10^6 and 3×10^8 cm s^{-1}. Since the dimensionless ionization parameter $\mathcal{U} = q/c$, this corresponds to $-3.5 < \log \mathcal{U} < -2.0$. Photoionization by power-law ionizing radiation produce identical line ratios to the shock models.

4.3.3. *Starburst-AGN Mixing*

Just as we have established a theoretical upper limit to the starburst activity on the diagnostic diagrams, we now establish a lower limit to starburst and AGN mixing.

To find the 100% AGN position of the mixing limit, we have used the shock model created using MAPPINGs which obtains the maximum magnitude in [N II] λ6584/Hα for the [N II] λ6584/Hα versus [O III] λ5007/Hβ diagram, [S II] $\lambda\lambda$6717,31/Hα for the [S II] $\lambda\lambda$6717,31/Hα versus [O III] λ5007/Hβ diagram, or [O I] λ6300/Hα for the [O I] λ6300/Hα versus [O III] λ5007/Hβ diagram. Due to the ionization parameter-metallicity degeneracy in these models and the differing sensitivity of each of the line ratios on the diagrams to shock excitation, the metallicity and ionization parameter for this maximum shock model vary from diagram to diagram. The position of this maximum shock model is the furthest to the right in the diagnostic diagrams as we can obtain with shock + ionizing precursor modeling within the realistic range of metallicity and ionization parameter.

Similarly, we find the 100% starburst point of the mixing limit as the photoionization model which produces the lowest and farthest to the right point on each diagnostic diagram.

The extreme mixing line joins the 100% starburst point and the 100% AGN point. This is a curve because of the log-log scale used in the diagrams.

Galaxies lying above and to the left of this extreme mixing line may be excited by a number of mechanisms which produce hard ionizing radiation fields. Such a radiation field may result from shocks due to stellar winds, accretion disks, or cooling flows. Alternatively, it may result from photoionization by a power-law ionizing radiation field associated with an AGN. Additionally, there may be mixing with photoionization due to starburst activity in the galaxy.

Galaxies lying below and to the right of the extreme mixing line cannot be modeled by either photoionization models or shocks with ionizing precursors. Galaxies in this region can be modeled by pure shocks without an ionizing precursor, or a power-law ionizing radiation field with an extremely low ionization parameter. As a result, our extreme mixing line provides a means to classify objects which are purely shock driven, and as a means to classify candidates for mixed excitation.

We can see from the mixing line that optical diagnostic diagrams are particularly sensitive to the presence of an AGN. Objects with as little as 20% AGN contribution to their energy budget may be classed as "AGN" using these diagnostics. Note, the same applies to objects classed using the VO87 empirical line.

4.4. *Starburst and AGN Classification*

Galaxies are classified as starbursts if they lie below and to the left of the theoretical maximum starburst line, and as AGNs if they lie above and to the right of the theoretical line. Galaxies which lie within 0.1 dex of the line are classed with an additional "borderline" criterion to represent the error estimate in our modeling. Galaxies which lie within this borderline region on two or more of the diagnostic diagram have been labeled as "possible composite" in Table 4 because they lie in between the starburst and AGN regions of the diagrams. We note that many of the objects in our sample appear to lie in between the starburst and AGN regions along a curve similar to that of the mixing line in the [N II] λ6584/Hα versus [O III] λ5007/Hβ and [O I] λ6300/Hα versus [O III] λ5007/Hβ diagrams. As many infrared galaxies have been found to be of composite nature in previous studies (e.g., Mazzarella et al. 1994; Genzel et al. 1998; Bransford et al. 1998; Scoville et al. 2000) it is likely that these galaxies lie on a "mixing sequence" containing both starburst and AGN phenomena. Alternatively, these galaxies may be excited by a slightly softer ionizing radiation field than the standard AGN due to weak shock or AGN activity.

Galaxies which fall within the AGN region on one or two diagrams and the starburst region on the remaining diagram(s) have been given ambiguous classifications. Fourteen galaxies (6%) are of this type. These galaxies may be very low-metallicity AGNs galaxies (if such objects exist), or composite starburst/AGN galaxies in which a large amount of the emission is due to star formation (Hill et al. 1999).

Due to our long-slit spectroscopy, we have been able to obtain multiple spectra and line ratios for 19 galaxies. These spectra are produced in separate line-emitting regions of these galaxies and may result from the presence of multiple nuclei. The majority of these galaxies have starburst spectra for each line-emitting region and have therefore been classified as starbursts, except for IRAS 01159−4443, IRAS 14575−2615, IRAS 15437+0234, IRAS 16399−0937, IRAS 21052+0340, and IRAS 23157−0441. The galaxies IRAS 01159−4443 and IRAS 14575−2615 have possible composite classification, while IRAS 15437+0234, IRAS 16399−0937, IRAS 21052+0340, and IRAS 23157−0441 contain both AGNs and starburst emission regions and are classed as composites. These galaxies are described in further detail in the Appendix.

Table 4 shows the classifications of our sample. The [S II] $\lambda\lambda$6717,31/Hα ratio is affected by density of the line emitting region, and therefore the [S II] $\lambda\lambda$6717,31/Hα versus [O III] λ5007/Hβ diagram may not be as accurate in classifying galaxies as remaining diagrams. In previous low-resolution studies, the blending of the [N II] and Hα lines often led to difficulties in classification. Our high-resolution spectra enable us to properly separate these lines so that [N II] λ6584/Hα versus [O III] λ5007/Hβ can be used as an accurate diagram for classification.

Dopita et al. (2000) has shown that instantaneous starburst modeling has had problems reproducing the [O I]

TABLE 4

SAMPLE CLASSIFICATIONS

This table is available only on-line as a machine-readable table

observations of H II regions (Dopita et al. 2000). This uncertainty may be due to the presence of shock excitation from mechanical energy transfer to stellar winds and supernovae (Dopita 1997; Stasińska & Leitherer 1996). However, we find that the continuous starburst models we have used here reproduce the [O I] observations of our sample quite well. We conclude from this that the presence of shock excitation from mechanical energy transfer of stellar winds and supernovae does not affect the [O I] flux in warm infrared starbursts sufficiently to cause such a problem.

4.5. *LINER Classification*

Objects falling below and to the right of the extreme mixing line are classed as LINERs and cannot be modeled by standard photoionization, radiative shocks or a mixture of the two. As noted earlier, the [S II] $\lambda\lambda$6717,31/Hα ratio is affected by density of the line emitting region, and therefore the [S II] $\lambda\lambda$6717,31/Hα versus [O III] λ5007/Hβ diagram may not be as accurate in classifying galaxies as the remaining diagrams. We also note that the [O I] λ6300/Hα versus [O III] λ5007/Hβ diagram appears to be the most accurate means to classify LINERs as the [O I] λ6300/Hα is the most sensitive to shocks. This is discussed in further detail in § 5.2. Objects lying within 0.1 dex to the right and below the extreme mixing line were given an AGN/L class as they are in between AGN and LINER regions on the diagram.

The ionizing source of LINERs is currently a hot topic of debate (see Filipenko 1989 for a review) and has been attributed to either collisional ionization by fast shocks (Taniguchi et al. 1999; Lutz et al. 1999; Dopita & Sutherland 1995; Veilleux et al. 1995) or photoionization by hot stars (Terashima et al. 2000). In many of these studies, LINERs have been classified using either the Heckman (1980) criteria of [O II] λ3737/[O III] λ5007 $\geq$ 1 and [O I] λ6300/[O III] λ5007 $>$ 1/3 or the Veilleux et al. (1995) criterion of log ([O III] λ5007/Hβ) $\leq$ 0.5. The Veilleux et al. (1995) criterion has been used in most of these studies because measurements of [O II] λ3737 were unavailable. As we can see from Figures 3*a* and 3*c* in particular, the Veilleux et al. (1995) selection criterion includes many of the objects which follow the curve of a possible starburst-AGN mixing sequence. These objects may composite galaxies, low-power AGN, or weak shocks with ionizing precursors and are most likely different in nature to the LINERs classed using our extreme mixing line. The LINERs classed using our extreme mixing line fall in the region of the diagnostic diagram corresponding to either photoionization by a hard radiation field with a very low ionization parameter (Veilleux & Osterbrock 1987) or emission by fast shocks in a gas-poor environment without an ionizing precursor. The fast shocks may be due to one or a combination of the following; superwind activity (Taniguchi et al. 1999; Kim, Veilleux, & Sanders 1998), cooling flows (Dopita et al. 1997), or a shocked accretion disk around an AGN (Dopita et al. 1997).

4.6. *Classification Using VO87 Diagnostics*

In order to compare the classification using our theoretical extreme mixing line and extreme starburst line with the semiempirical method of VO87, we have classified our galaxies according to the VO87 scheme. Following VO87 and Veilleux et al. (1995, hereafter V95), we classified galaxies above and to the right of the semiempirical line with [O III] λ5007/Hβ $>$ 3 as AGNs. Galaxies lying below and to the left of the semiempirical line are classed as starbursts, and galaxies lying to the right and with [O III] λ5007/Hβ $<$ 3 were classed as LINERs. These VO87 scheme classifications are presented in Table 4.

5. RESULTS

5.1. *Classification Statistics*

Statistics based on our theoretical classification scheme and with the VO87 classification scheme are shown in Table 5. We find 70% are starbursts, 4% Seyfert 1, 17% Seyfert 2, 0.4% LINERs, and 2% are composites. A fraction (20%) of the Seyfert galaxies, 3% of the starburst galaxies and (71%) of the ambiguous galaxies are possibly composite in nature also. We find 6% of the galaxies in our sample have ambiguous classification.

Using the VO87 classification method, we find 58% are starbursts, 4% Seyfert 1, 14% Seyfert 2, 6% LINERs, and 2% are composites. Using this scheme, we obtain ambiguous classifications of 16%.

The difference between the classification schemes is clear. Our theoretical method produces fewer ambiguous classifications and therefore is more consistent with classifying excitation from diagram to diagram. We also find fewer LINERs and more starbursts and AGN. Some of these starbursts and AGNs are possibly composite objects. A study of these possible composite objects and whether they are indeed starburst-AGN mixed excitation galaxies will be the topic of a future study.

To compare our classification results with other studies, the effects of selection criteria of the various samples must be taken into account. Far-infrared luminosity selection criteria will result in the fraction of AGNs detected increasing with higher infrared energy ranges for the sample. Similarly, the warmer the sample, the larger the number of AGNs that

TABLE 5

GLOBAL STATISTICS FOR THE 225 GALAXIES OBSERVED

	VO87 METHOD		THEORETICAL METHOD					
CLASS	Number	% of Sample	Number	% of Sample	$F_{60}/F_{25} < 6$ (%)	$F_{60}/F_{25} < 5$ (%)	$F_{60}/F_{25} < 4$ (%)	$F_{60}/F_{25} < 3$ (%)
Starbursts	129	58	157	70	51	39	27	23
AGN	40	18	46	21	46	59	73	77
Seyfert 2	31	14	37	17	…	…	…	…
Seyfert 1	9	4	9	4	…	…	…	…
LINERs	13	6	1	0.4	…	…	…	…
Composite	5	2	5	2	…	…	…	…
Possibly Composite			24	11	…	…	…	…

NOTE.—The AGN classification includes Seyfert 1 and Seyfert 2 objects. Multiple objects with an AMB classification were not included in these statistics.

will be detected. We observe that warm samples contain smaller numbers of LINERs than samples without color selection criteria. This is consistent with the scenario wherein LINERs are ionized by shocks without an ionizing precursor.

The study of very warm infrared galaxies ($3 \leq F_{25\,\mu m}/F_{60\,\mu m} \leq 1.5$) by de Grijp et al. (1992) found 37% starbursts, 22% Seyfert 1 galaxies, and 39% Seyfert 2 galaxies. The larger fraction of Seyferts found in the de Grijp study is a result of the very warm infrared color selection criterion used. The de Grijp et al. (1992) study found only a few LINERs out of 358 objects, consistent with the number of LINERs found here.

A study of a large sample of luminous infrared galaxies ($L_{IR} > 3 \times 10^{10}\ L_{\odot}$) was carried out by Kim et al. (1995) and classifications presented in Veilleux et al. (1995). They found 59% of their objects were starburst, 2% Seyfert 1, 12% Seyfert 2 and 27% LINERs. Our results for starbursts and Seyferts are similar to these, particularly for the VO87 classifications, although we find a lower percentage of LINERs. This is mostly due to the different methods used for LINER classification. Veilleux et al. (1995) used the log ([O III] λ5007/Hβ) $\leq$ 0.5 cutoff to class their LINERs, as originally suggested by Heckman et al. (1981). In our sample, we classify these as starburst or AGN galaxies including some with possible composite type. The remaining difference between the percentage of LINERs detected in our sample compared with the Veilleux et al. (1995) sample is probably a result the warm color selection criterion differences.

5.2. *Effect of the Warm Selection Criterion*

To test the effects of the warm selection criterion on our classifications, we used the line ratios from the *IRAS* Bright Galaxy sample of V95 on the diagnostic diagrams. To check the effect of selecting infrared galaxies on the LINER class, we also used the line ratios from the spiral galaxies classified as LINERs by Keel (1983). The diagnostic diagrams showing the V95 and Keel objects are shown in Figure 4.

Our galaxies occupy similar regions of the diagnostic diagrams to that of V95, and we therefore conclude that the effect of color selection is minimal on the position of the galaxies in the diagnostic diagrams.

Comparing the V95 LINERs to the Keel LINERs, we see that they both lie in a similar region of the [N II] λ6584/Hα versus [O III] λ5007/Hβ diagram but differ remarkably in the [S II] $\lambda\lambda$6717,31/Hα versus [O III] λ5007/Hβ diagram, and even more so in the [O I] λ6300/Hα versus [O III] λ5007/Hβ diagram. In the [S II] $\lambda\lambda$6717,31/Hα versus [O III] λ5007/Hβ diagram most of the Keel LINERs lie to the right of our extreme mixing line, while in the [O I] λ6300/Hα versus [O III] λ5007/Hβ diagram, all of them do. Whereas the V95 LINERs tend to occupy the region between starburst and AGN classification on the diagrams. One explanation for this is that selecting for infrared galaxies selects preferentially for objects of mixed excitation class.

It is clear that the best diagram for selecting LINERs with similar excitation to those in the Keel sample is the [O I] λ6300/Hα versus [O III] λ5007/Hβ diagram. This may be because [O I] λ6300 is more sensitive to the presence of shock excitation from mechanical energy transfer to stellar winds and supernovae (Dopita 1997; Stasińska & Leitherer 1996).

5.3. *Obscured AGN*

Seyfert 1 and 2 galaxies are most likely to be related via the "unified model" according to which orientation effects determine into which Seyfert class a galaxy will fall. The cause of the orientation effect is generally believed to be a geometrically and optically thick dusty molecular torus, which, for Seyfert 2 classed galaxies, obscures the AGN from direct view, but remains optically thin in the polar directions. As a result, spectropolarimetry provides a good means for finding "hidden broad-line regions" (HBLRs) in Seyfert 2 galaxies.

A number of the Seyfert 2 galaxies in our sample have been shown to contain HBLRs with spectropolarimetry; NGC 7674 contains a HBLR from optical spectropolarimetry (Miller & Goodrich 1990; Axon et al. 1994; Tran 1995). The infrared spectrum of this galaxy was studied by Veilleux et al. (1997), who argue that the broad base in the infrared Balmer lines are due to emission from a NLR rather than a genuine BLR. Optical spectropolarimetry shows a HBLR in IC 5063 (Inglis 1993). This galaxy has also been shown to contain a HBLR seen in the infrared regime (Heisler et al. 1997). Optical spectropolarimetry was also used by Tran, Miller, & Kay (1992) to uncover a HBLR in NGC 7212. IRAS 05189−2524 also contains a hidden broad-line region discovered through spectropolarimetry. Young et al. (1996) fitted two narrow components to each narrow emission line and a broad Hα to the red spectropolarimetric profile of this galaxy, classing it as a Seyfert 2. This galaxy has also been shown to contain broad Paα emission in the infrared (Veilleux, Sanders, & Kim 1999). In our spectra, The Hβ line is only seen in absorption in this galaxy, indicating an old stellar population. However, the strength of the [N II] λ6584, [S II] $\lambda\lambda$6717,31 lines indicate Seyfert activity.

The infrared regime provides another means to find HLBRs. It has been found that Seyfert 2 galaxies with warm infrared colors are more likely to harbor HBLR at near-infrared wavelengths (Veilleux, Goodrich, & Hill 1997; Dopita et al. 1998; Veilleux, Sanders, & Kim 1999). Our warm selection criterion should allow HBLRs to be observed in the infrared for many of our Seyfert 2 galaxies. IRAS 02304+0012 may have a weak HBLR in the infrared (Heisler & De Robertis 1995), although this is yet to be confirmed. A hidden AGN in NGC 3281 has been detected in both the infrared and X-ray regimes (Simpson 1998). Veilleux, Sanders, & Kim (1999) found a HBLR in IRAS 12071−0444 in the near-infrared and similarly for IC 3639 (Heisler, Lumsden, & Bailey 1997).

Other methods for discovering an obscured AGN include X-ray and radio techniques. For example, NGC 2110 has been found to contain a hidden AGN on the basis of X-ray spectroscopy (Malaguti et al. 1999).

NGC 1068 has been studied extensively and is well known to contain a HBLR. This has been confirmed at many different wavelengths (see, e.g., Antonucci & Miller 1985; Miller, Goodrich, & Mathews 1991; Young et al. 1995; Alexander, Young, & Hough 1999).

NGC 5506 has been reported to contain weak broad-line emission by Boisson & Durret (1986), who observed the presence of a broad Hα in her optical spectrum. This conclusion supports that of Shuder (1980), who also used a broad Hα in the optical line profile fitting. Morris & Ward (1985) argued for the presence of a hidden AGN based on

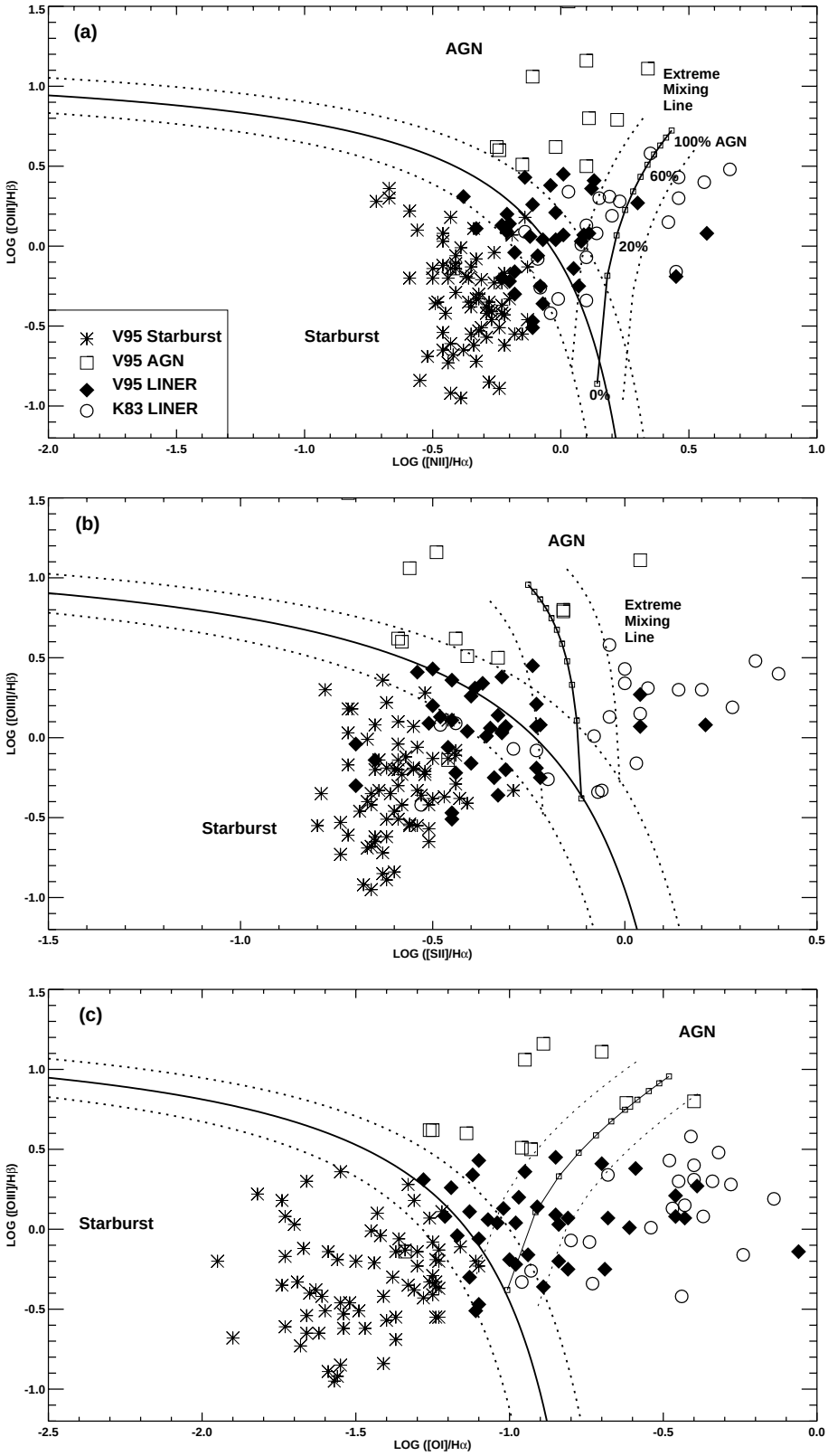

FIG. 4.—Diagnostic diagrams showing the galaxies in the Veilleux et al. (1995) bright galaxy sample and the LINERs in Keel (1983). Symbols for each object type are shown in the key in (*a*). Our theoretical classification line and extreme mixing line are shown in bold; dashed lines represent ± 0.1 dex of these lines, indicating the error range of our modeling.

the existence of the [O I] λ8446 emission line which is likely to reside in the broad-line clouds in active galaxies. Morris & Ward (1985) did not observe broad Balmer lines in their low-resolution spectrum. On the other hand, Veron et al. (1980) and Veilleux (1991) argue against the existence of broad Balmer lines in their optical spectra. Similar discrepancies exist in the infrared regime for this galaxy, with the presence of broad infrared Paβ reported by Blanco, Ward,

& Wright (1990), Rix et al. (1990) and Ruiz, Rieke, & Schmidt (1994). However, Veilleux et al. (1997) argue against the presence of broad Balmer lines in the infrared regime and suggest that the Balmer line profiles result, rather, from are strong, highly reddened emission in the wings of the lines. NGC 5506 has been previously classed as a Seyfert 1.9 (Mazzarella & Balzano 1986) and a Seyfert 1 by Kewley et al. (2000). We note that the [N II] and Hα emission-line profile is equally well fitted by either of two scenarios. In the first scenario, we fitted a broad Hα plus narrow emission lines to each of Hα, [N II] λ6584, and [N II] λ6548 emission lines (Seyfert 1 profile). In the second scenario we fitted each emission line by two Gaussians, composing one narrow Gaussian and a broad, slightly blue-shifted Gaussian to account for the for the broad base and wings of the lines (Seyfert 2 profile). We find that the second scenario of fitting each emission line with two Gaussians produces a better fit to the remaining emission lines than just a single Gaussian. We therefore prefer to allocate this galaxy a Seyfert 2 classification until higher resolution spectroscopy becomes available.

5.4. *Infrared Colors*

The line ratio [O III] λ5007/Hβ is plotted against the infrared color index F_{60}/F_{25} in Figure 5. Galaxies classed as AGNs (*filled circles*), starbursts (*crosses*), and composite/possible composite (*open circles*) objects are shown. The vertical separation between AGNs and starbursts is merely a result of classification using the theoretical classification line on the diagnostic diagrams. As expected, AGNs have on average a warmer F_{60}/F_{25} ratio than starbursts, but they cover a wider range ($3 < F_{60}/F_{25} < 8$) of colors than do starbursts ($\sim 4 < F_{60}/F_{25} < 8$). The cooler AGNs (i.e., those with $\sim 4 < F_{60}/F_{25} < 8$) generally have lower [O III] λ/Hβ ratios and these galaxies lie on the mixing sequence between starburst and AGN on Figure 3. The percentage of galaxies classed as starburst and AGN for FIR colors greater than 3, 4, and 5 are shown in Table 5. The scarcity of objects having H II region–like [O III] λ5007/Hβ ratios and very warm F_{60}/F_{25} ratios shows that there are very few AGNs which have entirely dust obscured narrow-line regions. In the context of the unified model of AGN, this implies that in most cases, the AGN succeeds in pushing an "ionization cone" through the very dense circumnuclear gas. If the Sanders et al. (1988b) merger scenario exists, then one would expect an evolution in Figure 5 shown by a hypothetical mixing line from the lower right-hand corner of pure starburst activity to the central region of the diagram which represents starburst and AGN mixing, and finally to the top left-hand corner of pure AGN activity. It is clear that many of our AGNs can fit onto such a mixing line. Note, this hypothetical mixing line is not related to our theoretical extreme mixing line on the diagnostic diagrams.

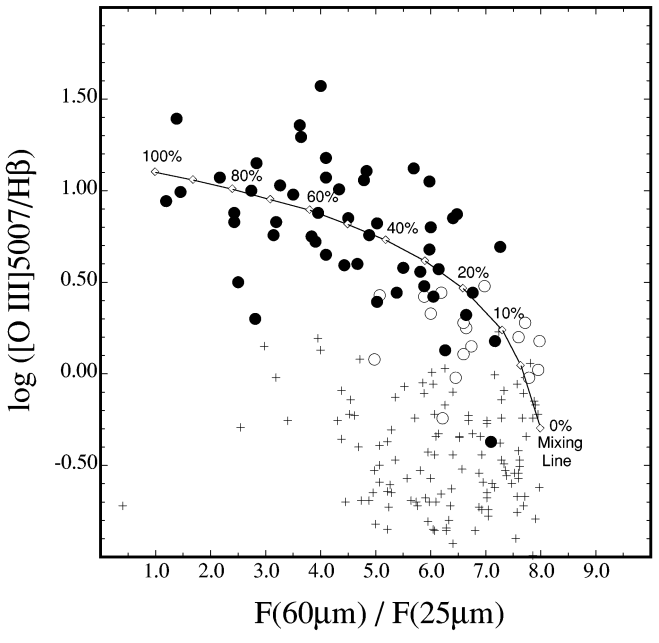

FIG. 5.—Diagram of the infrared color ratio $F_{60\,\mu m}/F_{25\,\mu m}$ vs. [O III]/Hβ for objects with log ([N II λ6584/Hα) > 0.5. Galaxies classed as starbursts (*crosses*), AGNs (*filled circles*), and ambiguous classification (*unfilled circles*) using Fig. 3 are shown. The AGN class for the purposes of this diagram includes the one LINER in our sample. Most of the AGNs appear to follow the curve of the hypothetical mixing line. This line is not related to the theoretical extreme mixing line shown in Figs. 3 and 4.

5.5. *FIR Luminosity*

Figure 6 shows the diagnostic diagram of [N II] λ6584/Hα versus [O III] λ5007/Hβ with galaxies in the IR luminosity ranges $L_{IR} < 10^{10}\ L_\odot$ (*circles*), $10^{10}\ L_\odot < L_{IR} < 10^{11}\ L_\odot$ (*asterisks*), and $10^{11}\ L_\odot < L_{IR} < 10^{12}\ L_\odot$ (*squares*) marked. We can see that galaxies with $L_{IR} < 10^{10}\ L_\odot$ are generally pure starbursts or low-luminosity AGN. There is little evidence for mixed excitation. Galaxies with $10^{10}\ L_\odot < L_{IR} < 10^{11}\ L_\odot$ cover the entire range of starburst and AGN activity or mixtures of the two. Galaxies with $10^{11}\ L_\odot < L_{IR} < 10^{12}\ L_\odot$ appear to lie predominantly in the region between starburst and AGN along a curve similar to our mixing line in Figures 3 and 4. These results are consistent with the merger scenario of luminous infrared galaxies (Sanders et al. 1988b). In this scenario, an interaction between two galaxies would be initially accompanied by

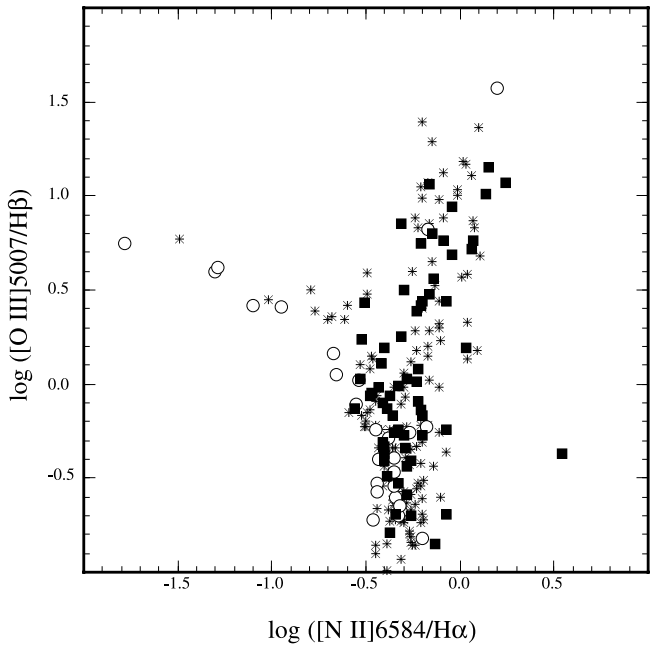

FIG. 6.—Diagnostic diagram of [N II] λ6584/Hα vs. [O III] λ5007/Hβ showing galaxies in the IR luminosity ranges $L_{IR} < 10^{10}\ L_\odot$ (*circles*), $10^{10}\ L_\odot < L_{IR} < 10^{11}\ L_\odot$ (*asterisks*), and $10^{11}\ L_\odot < L_{IR} < 10^{12}\ L_\odot$ (*squares*).

vigorous star formation triggered by tidal interactions, and resulting in strong FIR radiation from heated dust. In the late stages of the merger, gas from the merging galaxies may be accreted to the central regions to power an AGN (Barnes & Hernquist 1996), further increasing the IR luminosity. Finally, the tidal interactions subside, causing the contribution to FIR by star formation to decrease (hence decreasing the IR luminosity) and the line ratios will be dominated by the AGN. According to our results, if this merger scenario holds, then the FIR luminosity increases from 10^{10}–10^{11} $L_{\odot}$ to 10^{11}–10^{12} $L_{\odot}$ or higher when intense star formation is triggered and AGN mixing begins. During this stage, the starburst moves from the starburst region on the diagnostic diagrams up the mixing sequence toward the AGN region as the AGN contribution to the overall energy budget increases. Once the tidal interactions and hence the intense starburst activity subsides, the IR luminosity may decrease to less than 10^{10} $L_{\odot}$ and the line ratios show a pure AGN. However, this scenario must remain tentative until the effects of the intrinsic galaxy luminosity and starburst age can be definitely separated. The attempt to do this will be the subject of a future paper.

5.6. *Blue Asymmetry Galaxies*

We have 16 galaxies in our sample which show blue asymmetries in their line profiles. As mentioned earlier, asymmetries in the [O III] λ5007 line have been extensively studied by Whittle (1985) and Heckman et al. (1981). NGC 7674 contains a very strong blue asymmetry in its spectrum which has been studied extensively (e.g., Shuder & Osterbrock 1981; Feldman et al. 1982; de Robertis & Osterbrock 1986; Veilleux 1991; Veilleux et al. 1999). The blue asymmetry is has been tentatively linked to regions of high ionization/critical density (de Robertis & Shaw 1990). Many of the galaxies in our sample which display a blue asymmetry show larger asymmetries on the higher ionization emission lines, supporting this.

It is most likely that the blue asymmetries result from outflows of gas with distributed opaque clouds. It is also possible that inflow of gas with opaque clouds internal to the narrow-line emitting region could produce the blue asymmetry. Studies of H I absorption and the velocity field of the absorbing region have found that both inflows and outflows occur in narrow-line emission galaxies (see, e.g., Mirabel 1982 and Heckman et al. 1981). Alternatively, the asymmetries may arise from separate regions of line emitting gas, with different gas velocities.

The majority (69%) of the galaxies with blue asymmetries presented here are of AGN type, with 63% Seyfert 2 and 6% Seyfert 1. A further 25% are starbursts and one is of ambiguous classification. Compared with the statistics of our whole sample, we can see that blue asymmetries may be a good indicator of AGN activity, and the blue asymmetry may be a result of gas flowing radially away from or toward the AGN core. We find that the average electron density of these galaxies is $\sim$600 cm^{-3} compared with an average of $\sim$350 for our entire sample. This is consistent with the majority of these being AGNs with dense gas flows toward or away from the nucleus.

The average F_{60}/F_{25} for these blue asymmetry galaxies is 4.8 compared with 6.4 for our whole sample. This is consistent with the majority AGN class, as AGN galaxies are well known to have warmer infrared colors than starburst galaxies, in general. Similarly, the average infrared luminosity is $L_{\rm IR} \sim 10^{11.2}$, higher than the average of $L_{\rm IR} \sim 10^{10.8}$ for our whole sample. This is consistent with the AGN classification as the fraction of AGN is known to be correlated with the infrared luminosity.

6. SUMMARY

We have presented the optical spectroscopy for 225 warm infrared galaxies in our sample ($10^{8} < L_{\rm IR} < 10^{12.5}$ $L_{\odot}$). We have classified these galaxies using the standard optical line ratios [N II] λ6584/H α versus [O III] λ5007/Hβ, [S II] $\lambda\lambda$6717,31/Hα versus [O III] λ5007/Hβ, and [O I] λ6300/Hα versus [O III] λ5007/Hβ. The region of diagnostic space occupied by starbursts has been derived from detailed modeling and has been used to separate the galaxies into starburst or AGN type objects. The LINER region defined here excludes the objects of possible composite (AGN + starburst) nature by use of a theoretically derived extreme mixing line obtained from our modeling. We compared the optical classifications with infrared colors and analyzed the position of the different classes of FIR luminosity on the [N II] λ6584/Hα versus [O III] λ5007/Hβ diagnostic diagram. The main conclusions of the analysis are as follows.

1. We find that 70% of the galaxies studied are H II region–like or starbursts, 17% are Seyfert 2, 4% are Seyfert 1, and 2% are composite. This is consistent with previous samples of luminous infrared galaxies, taking into account the selection effects on each sample.

2. Our theoretical method for classification results in 6% ambiguous galaxy classifications compared with 16% obtained using the VO87 method. This implies strongly that our method is more consistent in classifying the excitation between the three optical diagnostic diagrams.

3. Many of the galaxies in our sample appear to lie on a mixing sequence between starburst and AGN. A number of these galaxies would have previously been classed as LINERs if we were to use the V95 selection criterion of log ([O III] λ5007/Hβ) $\leq$ 0.5.

4. LINERs classed using our extreme mixing line may be due to either or a combination of ionization by a hard radiation field with a low-ionization parameter or fast shocks without an ionizing precursor. The fast shocks may be associated with either superwinds from intense star formation, an accretion disk around an AGN, or cooling flows. Warm samples appear to select against LINERs.

5. The [O I] λ6300/Hα versus [O III] λ5007/Hβ diagnostic diagram is the most sensitive to the excitation in LINERs, and it shows that infrared selected galaxies contain LINERs of different levels or types of excitation than non–infrared-selected samples.

6. Galaxies with $L_{\rm IR} < 10^{10}$ $L_{\odot}$ are generally starburst or AGN with little mixing. Galaxies with 10^{10} $L_{\odot} < L_{\rm IR} < 10^{11}$ $L_{\odot}$ cover the entire range of starburst and AGN activity. Galaxies with 10^{11} $L_{\odot} < L_{\rm IR} < 10^{12}$ $L_{\odot}$ appear to be predominantly composite galaxies with various degrees of starburst-AGN mixing.

7. AGNs in our sample cover a wider range ($3 < F_{60\,\mu{\rm m}}/F_{25\,\mu{\rm m}} < 8$) of infrared colors than do starbursts ($\sim 4 < F_{60\,\mu{\rm m}}/F_{25\,\mu{\rm m}} < 8$). As found in previous studies, the percentage of AGNs increases with warmer infrared colors. Objects classified as starbursts with warmer infrared colors ($F_{60\,\mu{\rm m}}/F_{25\,\mu{\rm m}} < 4$) are possible candidates for dust-obscured AGNs, but these are quite scarce in our sample.

8. Our sample contains 16 galaxies with blue asymmetries to their optical line profiles. These galaxies are mostly of AGN type, have higher average IR luminosity, are warmer than average infrared colors, and are denser than the average for that our entire sample. These galaxies are most likely to be AGNs with radial flows of dense gas toward or, most likely, away from the nucleus.

Further analysis of these spectra will be published in forthcoming papers.

We wish to thank the referee for his helpful and thorough comments. We would like to thank the staff at Siding Springs Observatories for their assistance during our spectroscopy observations. This research has made use of the NASA/IPAC Extragalactic Database (NED), which is operated by the Jet Propulsion Laboratory, California Institute of Technology, under contract with the National Aeronautics and Space Administration.

APPENDIX

NOTES ON INDIVIDUAL OBJECTS

IRAS 00163−1039 (*Arp 256*).—We have extracted spectra for three emission knots in this galaxy. All three knots are H II region–like objects with different line profiles. These objects are aligned along an axis 165° to the N. Object 1 is at distance of $\sim 1'$ from object 2. Object 2 is at a distance of $\sim 9''$ from object 3. This galaxy is the merger of two spirals MCG -2-1-51 and MCG -2-1-52 (Dahari 1985; Martin et al. 1991) which have been found to be separated by 1′ in NS direction by Martin et al. (1991). Object 1 in our study corresponds to MCG -2-1-51, while objects 2 and 3 most likely correspond to separate line emitting regions in MCG -2-1-52.

IRAS 00198−7926.—We classify this object as a Seyfert 2, supporting its previous classification as a Seyfert 2 by Allen et al. (1991). The [O III] lines in this galaxy have a slightly larger FWHM (~ 500 km s^{-1}) than the remaining narrow emission lines (~ 250 km s^{-1}) and were therefore fitted with wider Gaussians.

IRAS 00344−3349.—We extracted the spectra from two line-emitting objects in this galaxy. Both are H II region–like with very similar line profiles. These objects are aligned east and are separated by $\sim 5''$. This galaxy has been found previously to contain three nuclei, all of which are H II region–like objects (Heisler & Vader 1994, 1995). Our spectra correspond to two of these three nuclei.

IRAS 01050−3305.—We have obtained spectra for IRAS 01050−3305 (object 2) and a second galaxy $\sim 45''$ from IRAS 01050−3305 aligned 260° from N (object 1). The Digitized Sky Survey (DSS) image for IRAS 01050−3305 clearly shows the two galaxies separated by 40″–50″. Both of these galaxies are H II region–like with different line profiles, and notably different line widths. We find that both IRAS 01050−3305 and the second galaxy are at a redshift of 0.036 ± 0.005 and are possibly interacting.

IRAS 01159−4443.—We have obtained spectra for the two nuclei of this (previously known) interacting galaxy (Condon 1996). These nuclei are aligned *NS* and are separated by $\sim 20''$. Nucleus 1 is H II region–like, and nucleus 2 is a possible composite galaxy. These correspond to the northern nucleus (nucleus/object 2) and the southern nucleus (nucleus/object 1) described by Condon et al. (1996).

IRAS 01341−3734 (*NGC 633*).—We have obtained spectra for both galaxies of this interacting pair (Telesco, Wolstencroft, & Done 1988; Johansson & Bergvall 1990). We find the northern spiral galaxy, NGC 633 (object 1) is separated from the southern elliptical galaxy MGC-06-04-057 by $\sim 70''$ along a position axis (PA) of 171°. We find that both objects are H II region–like and display similar line ratios. Condon et al. (1996) notes that the position of the *IRAS* source suggests that both galaxies contribute significantly to the *IRAS* source.

IRAS 03229−0618 (*Mrk 0609*).—This galaxy contains broad Balmer lines and we class this galaxy as a Seyfert 1. Osterbrock (1981) classed this galaxy as a Seyfert 1.8; however, with our high-resolution spectroscopy, we can clearly observe broad Balmer lines in this galaxy. As noted by Veron, Goncalves, & Veron-Cetty (1997), IRAS 03229−0618 has [O III] lines which are about 4 times wider than the Hβ emission line. From our spectra, we can see that the [O III] lines contain a blue asymmetry as well as being about 4 times wider than the remaining emission lines, suggesting that the [O III] resides closer to the nuclear Seyfert than the remaining line-emitting gas and that there are radial flows of the line-emitting gas. The [O III] lines were well fitted by a narrow component plus a blueshifted broad component. The combined flux of these components was used to determine the [O III]λ 5007/Hβ line ratio.

IRAS 03536−1351.—This galaxy has not been classed previously and we class it as a starburst. Its emission lines have a blue asymmetry, indicating radial flows of line-emitting gas. Blueshifted Gaussian components were fitted to all lines.

IRAS 03575−6132.—This galaxy is classed as a Seyfert 2 and its emission lines have a blue asymmetry, indicating radial flows of line-emitting gas. Blueshifted Gaussian components were fitted to Hα, [N II] λ6584, Hβ, [O III]λ 4959 and [O III]λ 5007. The S/N ratio was too low to fit blueshifted Gaussians to the remaining lines, and one narrow Gaussian was sufficient.

IRAS 04131−2836 (*NGC 1540*).—This object is a known galaxy pair (Corwin, de Vaucouleurs, & de Vaucouleurs 1985). We find two line emitting regions separated by $\sim 15''$ along a PA of 29°. Both of these regions are H II region–like with very similar line ratios. Due to the separation between these regions, they most likely correspond to two separate line emitting regions embedded in the northern galaxy of the pair.

IRAS 04259−0440.—We class this galaxy as a Seyfert 2. It has been classed previously as a Seyfert 2 (Vader et al. 1993) and a LINER type galaxy (Osterbrock & de Robertis 1985). Its emission lines show a blue asymmetry in the red indicating radial flows of the line-emitting gas. The line profiles were well fitted by a narrow Gaussian plus a broader, blueshifted Gaussian for each line. The fluxes used to determine the line ratios are composed of the sum of the narrow plus blueshifted components.

IRAS 04339−1028 (*MCG -02-12-045*).—This object shows very strong broad Balmer lines and is classed as a Seyfert 1. The [O III] lines are fitted well by a narrow and a broad component. The flux from these combined Gaussian components was used for the [O III]λ /Hβ line ratio.

IRAS 05189−2524.—This galaxy has a very complex line profile. It either has two narrow components to each narrow emission line and a broad Hα (Seyfert 1), or three components to each narrow emission line comprising two narrow components and a blueshifted broader component (Seyfert 2). The rms deviation of the Chi-square of the fit is very similar for both scenarios, and it is unclear from our spectra which is correct. The Hβ line is only seen in absorption, indicating an old stellar population. Young et al. (1996) carried out optical spectropolarimetry on this galaxy and fitted two narrow components to each narrow emission line and a broad Hα to the red spectropolarimetric profile of this galaxy, classing it as a Seyfert 2. Our line profile for the [N II] and Hα complex looks very similar to that of Young et al. (1996), so it is possible that we may be seeing the broad-line region in the optical for the first time; however, higher resolution optical spectroscopy is required to confirm this. This galaxy has also been shown to contain broad Paα emission in the infrared (Veilleux et al. 1999).

IRAS 05238−4602.—This galaxy is classed as a Seyfert 2 and its emission lines have a slight blue asymmetry, indicating radial flows of line-emitting gas. Blueshifted Gaussian components were fitted to all narrow emission lines.

IRAS 05409−2405.—This object is a known interacting pair (Telesco et al. 1988). The digitized sky survey image shows two interacting galaxies $\sim$30″ apart. We have obtained spectra for both of these galaxies. The galaxies have different line profiles, one which we classify as a starburst, the other we are unable to classify because the S/N ratio at blue wavelengths was too low to decompose [O III] λ5007 into a Gaussian. It is unclear to us which spectrum belongs to which galaxy of the pair.

IRAS 06259−4708.—This object is composed of four main galaxies of normal sizes and luminosities embedded in what looks like a common halo (Bergvall, Ekman, & Lauberts 1981). We have obtained spectra for the northern pair of these galaxies, corresponding to galaxies a and b in Bergvall et al. (1981). We find both objects are H II region–like with different line profiles and are separated by $\sim$14″.

IRAS 07027−6011.—This galaxy is classed as a Seyfert 2 and its emission lines have a blue asymmetry, indicating radial flows of line-emitting gas. Blue Gaussian components were fitted to each emission line of this galaxy.

IRAS 10042−2941 (*NGC 3125*).—We have obtained spectra for two emission line regions in this galaxy separated by $\sim$9″. The spectra for these are very similar and both lie in the starburst region of the diagnostic diagrams. Two knots of starburst activity have been found in this galaxy by Schaerer, Contini, & Kunth (1999) separated by $\sim$10″. Our spectra correspond to these two knots.

IRAS 10295−1831.—This galaxy is classed as an AGN using the [N II] λ6584/Hα versus [O III] λ5007/Hβ diagnostic diagram, as a H II/borderline galaxy using the [S II] $\lambda\lambda$6717,31/Hα versus [O III] λ5007/Hβ diagram, and as an AGN/borderline galaxy using the [O I] λ6300/Hα versus [O III] λ5007/Hβ. We have therefore assigned it within the "ambiguous" class of galaxies. The [O III] emission lines of this galaxy are broader (470 km s^{-1}) than the remaining optical emission lines ($\sim$230 km s^{-1}) and were therefore fitted with wider Gaussians. The line width suggests that it may well be an AGN.

IRAS 11083−2813.—We class this galaxy as a Seyfert 1, as it has strong broad Balmer lines. Its line profiles appear to have broad wings, particularly for the [O III] 5007 line. We fitted this line with an extra broad component to account for the broad wings.

IRAS 11365−3727 (*NGC 3783*).—This galaxy shows strong broad Balmer lines and we class it as a Seyfert 1. The [O III] lines are fitted well by a narrow component ($\sim$190 km s^{-1}) and a broader ($\sim$480 km s^{-1}) component. Only a narrow ($\sim$190 km s^{-1}) component is required to fit the remaining narrow emission lines.

IRAS 12071−0444.—We class this galaxy as a Seyfert 2. The red emission lines show a clear blue asymmetry which was fitted by an extra blueshifted broader component for each emission line. The combined flux for the narrow and blueshifted components were used to determine the line ratios. Due to the low S/N ratio in the blue, we were unable to fit a blueshifted Gaussian to Hβ or the [O III] lines.

IRAS 12329−3938 (*NGC 4507*).—We class this galaxy as a Seyfert 2. All emission lines show a clear blue asymmetry indicating radial flows of the line emitting gas. The line profiles were well fitted by a narrow plus broader blueshifted component to each emission line. The flux in these combined components was used to determine the line ratios.

IRAS 12540−4251 (*MCG -7-27-20*).—This galaxy is classed as an AGN using the [O I] λ6300/Hα versus [O III] λ5007/Hβ diagnostic diagram, as a H II/borderline galaxy using the [N II] λ6584/Hα versus [O III] λ5007/Hβ diagram and as a H II galaxy using the [S II] $\lambda\lambda$6717,31/Hα versus [O III] λ5007/Hβ. We therefore assign it with "ambiguous" classification. The emission lines show a blue asymmetry and are well fitted by a narrow plus a broader blueshifted Gaussian for each line. The combined flux from the narrow and blueshifted component was used to determine the line ratios.

IRAS 12596−1529 (*MCG -02-33-098*).—We find three emission knots in this galaxy, all of which are classified as H II region–like. These knots are along the axis of the galaxy (PA = 65°) each separated by $\sim$11″. This galaxy is an interaction between MCG -02-33-098 and MCG -02-33-099 and also has companions 0.5 and 0.8 to the north of MCG -02-33-098. (Vorontsov-Velyaminov & Arhipova 1968). Veilleux et al. (1995) obtained spectra for two objects in this galaxy, both of which were classed as H II region–like. It is unclear which of our spectra correspond to the two spectra obtained by V95 or the four companions mentioned by Vorontsov-Velyaminov & Arhipova (1968).

IRAS 13229−2934 (NGC 5135): We classify this galaxy as a Seyfert 2, supporting the classification by Vaceli et al. (1997). The narrow emission lines have a slight blue asymmetry and were well fitted by a narrow Gaussian plus a broader blueshifted Gaussian. The combined flux of these components was used to determine the line ratios.

IRAS 13336−0046.—We find three emission knots in this galaxy, all of which are classified as H II region–like. These regions are along the axis of the galaxy (131° to N). Objects 1 and 2 are separated by $\sim$37″, and objects 2 and 3 are separated by $\sim$12″. This galaxy has been previously classed as a galaxy triple by Nilson (1973).

IRAS 13370+0105 (*Arp 240*).—We find two emission knots in this galaxy separated by $\sim 76''$. The S/N ratio for these spectra is insufficient to allow us to classify these objects reliably; however, object 2 lies in the H II region of the [N II] λ6584/Hα versus [O III] λ5007/Hβ diagnostic diagram. This galaxy is a known interaction between NGC 5257 and NGC 5258 (Vorontsov-Velyaminov 1959). From the flux ratios given for NGC 5257 and NGC 5258 in Lui & Kennicutt (1995), these galaxies are classed as starbursts.

IRAS 14106−0258 (*NGC 5506*).—This galaxy has been previously classed as a Seyfert 1.9 (Mazzarella & Balzano 1986) and a Seyfert 1 by Kewley et al. (2000). NGC 5506 has been reported to contain weak broad-line emission (Boisson & Durret 1986; Morris & Ward 1985). On the other hand, Veilleux, Goodrich, & Hill (1997) argue against the existence of broad Balmer lines in the infrared regime. We note that the [N II] and Hα emission-line profile is well fitted by either broad Balmer lines plus narrow emission lines (Seyfert 1 profile), or by fitting each line by a narrow Gaussian plus a broad Gaussian for the broad wings with a slight blue asymmetry (Seyfert 2 profile), confusing the issue of Seyfert classification for this object. We find that fitting each emission line with two Gaussians, one narrow and one for the broad wings with a slight blue asymmetry produces a better fit to the remaining emission lines than a single Gaussian. We therefore prefer to allocate this galaxy a Seyfert 2 classification until higher resolution spectra becomes available for this galaxy. The combined flux of the two Gaussians per emission line was used to determine the line ratios in this case.

IRAS 14575−2615.—We find two line emission knots in this galaxy separated by $\sim 11''$ along a PA of 22°. Object 1 lies in the H II/B region of the [N II] λ6584/Hα versus [O III] λ5007/Hβ diagnostic diagram and in the AGN/B region of the remaining diagrams, and therefore we have assigned it an "ambiguous" classification. Object 2 is classed as H II region–like. This galaxy may be either of composite type or of high-metallicity starburst type. This galaxy is a known interacting pair of spiral galaxies (Winkler 1988). Our spectra correspond to the two line emitting regions in the northern galaxy of the pair. Winkler (1988) found two bright condensations in this northern galaxy, each of H II region type.

IRAS 15361−0313.—We class this galaxy as an "ambiguous" object. It appears to contain a redshifted broad Hα, and it lies in the AGN/B region of the [N II] λ6584/Hα versus [O III] λ5007/Hβ diagnostic diagram and in the H II/B region of the [S II] $\lambda\lambda$6717,31/Hα versus [O III] λ5007/Hβ diagram. The S/N ratio of the [O I] λ6300 line is insufficient to allow classification using the [O I] λ6300/Hα line ratio. This galaxy has been previously classed as a Seyfert 1.9 by Condon et al. (1998).

IRAS 15437+0234 (*NGC 5990*).—We find two objects in this galaxy separated by $\sim 8''$ along a PA of 144°. One of these objects is classified as an AGN (Seyfert 2), and the other is classified as a H II region. The H II region object is the stronger of the two, and thus IRAS 15437+0234 is dominated by its starburst in the optical. As it contains both AGNs and H II region–like spectra, we class this galaxy as a composite. This is a known galaxy pair (Nilson 1973) and is classed in the FIR as a starburst (Coziol et al. 1998).

IRAS 15456−1336 (*NGC 5955*).—This object shows a clear broad Hα and is classed as a Seyfert 1. The [O III] lines in the blue are broader than the remaining emission lines were well fitted by a narrow plus a broader component for each line. The combined flux of these two components was used to determine the [O III]/Hβ line ratio.

IRAS 16399−0937.—We find two objects in this galaxy separated by $\sim 7''$ along a PA of 177°. One of these objects is classified as an AGN (Seyfert 2), and the other is classified as a H II region. Both objects are similar in strength and we class this galaxy as a composite.

IRAS 17467+0807.—This galaxy has been previously classed as a starburst (Coziol et al. 1998), and our optical spectra support this result. Its emission lines have broad wings with a very slight blue asymmetry indicating radial flows of the line-emitting gas. The flux in each emission line was calculated using the sum of a narrow Gaussian and a broader Gaussian to account for the broad wings.

IRAS 18093−5744 (*IC 4687*).—We find two H II regions in this galaxy separated by $\sim 28''$ along a PA of 191°. This galaxy is interacting with IC 4686 and IC 4689 (West 1976). Our spectra correspond to IC 4686 (object 2) and IC 4687 (object 1). Durret & Bergeron (1988) suggest that a weak LINER is present in IC 4687 from the [O I] λ6300 line detected in their study at the 4 σ level. However, on the basis of our spectra at [O I] λ6300, this classification seems unlikely. Furthermore, the flux ratios for IC 4687 do not suggest any LINER activity from either the [N II] λ6584/Hα versus [O III] λ5007/Hβ or the [S II] $\lambda\lambda$6717,31/Hα versus [O III] λ5007/Hβ diagrams using either VO87 classification method or our theoretical method.

IRAS 18325−5926.—This galaxy has been classed previously as a Seyfert 2 (de Grijp et al. 1992), and our optical spectra support this classification. The emission lines have a broad base with a slight blue asymmetry. These were well fitted by a narrow Gaussian plus a broader slightly blue shifted Gaussian. The flux for these combined Gaussians was used to determine the line ratios.

IRAS 18429−6312 (*IC 4769*).—We class this galaxy as a Seyfert 2. The [O III] emission lines in the blue show a clear blue asymmetry and were well fitted by a narrow Gaussian plus a broader blue shifted Gaussian. The flux for these combined Gaussians was used to determine the [O III]/Hβ line ratio.

IRAS 19335−2011.—We find three line-emitting objects in this galaxy pair (Lauberts 1982) along a PA of −88°. From our spectra, objects 1 and 3 are classed as H II regions. The S/N ratio in the blue for object 2 is not sufficient for classification. Objects 1 and 2 are separated by $\sim 3''$ and objects 2 and 3 are separated by $\sim 6''$.

IRAS 20082+0058.—This galaxy has no previous classification, and we class it as a starburst. Its emission lines contain a blue asymmetry indicating radial flows of the line emitting gas. The emission lines were well fitted by a narrow component plus a broader blueshifted component. The combined flux from these components was used to determine the line ratios.

IRAS 21052+0340.—We have obtained spectra for the two galaxies of the interacting pair of spirals in this galaxy (Zwicky 1971). We find that the eastern galaxy (object 1) is of AGN (Seyfert 2) type, and the western galaxy (object 2) is H II region–like. These galaxies are separated by $\sim 71''$.

IRAS 21330−3846 (*MGC -7-43-17*).—We have obtained spectra for two line-emitting objects in this galaxy which are separated by $\sim 11''$ of 22°. Both objects are H II region–like using our theoretical diagnostics. This is a known interacting pair

(Vorontsov-Velyaminov & Arhipova 1974). van den Broek et al. (1991) finds two nuclei for this pair and classes the northern nucleus as a LINER/Seyfert 2 type and the southern nucleus as a H II region, similar to our findings using the VO87 classification method.

IRAS 22007+0019 (*NGC 7189*).—We classify this galaxy as an "ambiguous" object, as it lies within the starburst region of the [S II] $\lambda\lambda$6717,31/Hα versus [O III] λ5007/Hβ diagram, but within the AGN region of the remaining two. It has not been classified previously. This galaxy has much broader [O III] lines than the remainder of its narrow emission lines. The [O III] lines were well fitted by a narrow and a broader component. The combined flux of these Gaussians was used in the [O III] λ5007/Hβ ratio for classification. The width of the [O III] lines suggest the presence of an active nucleus.

IRAS 23128−5919.—We class this object as a starburst using both our theoretical classification scheme and the VO87 scheme. As it lies within the borderline region on two out of the three diagnostic diagrams, we have classed it as a possible composite. It has previously been classed as a starburst (Lutz et al. 1999), and a LINER (Young et al. 1996), and Duc, Mirabel, & Maza (1997) classed it is a mixture of LINER, Seyfert 2 and starburst activity. All emission lines for IRAS 23128−5919 galaxy have a blue asymmetry. These lines were well fitted by a narrow Gaussian and a broader, blueshifted Gaussian. The combined flux for these components was used to determine the line ratios.

IRAS 23157−0441 (*NGC 7592*).—We have obtained spectra for two objects in this galaxy separated by $\sim$12.″5 along a PA of $-79°$ to N. Object 1 is classed as an AGN (Seyfert 2) and object 2 is classed as a starburst. This system is a known interacting pair (Vorontsov-Velyaminov & Arhipova 1963) and has been studied in detail by Rafanelli & Marziani (1992). Our results confirm those of Rafanelli & Marziani (1992), who conclude that NGC 7592 contains both starburst and Seyfert activity. The line profile of Object 1 has a strong red asymmetry in the [O III] emission lines. We fitted an extra component to these lines and the combined flux of the narrow plus redshifted broader Gaussians was used in the [O III]/Hβ ratio.

IRAS 23254+0830 (*NGC 7674*).—We class this galaxy as a Seyfert 2. All lines display a strong blue asymmetry and were therefore fitted by a narrow component plus a broader blueshifted component. The flux of the combined components were used for classification.

IRAS 23262+0314 (*NGC 7679*).—This galaxy has optical emission line ratios typical of a H II region but contains a small broad Hα with FWHM of $\sim$2000 km s^{-1}. We class this as a composite galaxy. It has been previously classed as a Seyfert 2 by V95 and contains a circumnuclear starburst ring (Pogge & Eskridge 1993). It is most likely that our narrow emission line ratios are dominated by this starburst ring and that our high resolution is sufficient to also detect the broad-line region.

REFERENCES

Alexander, D. M., Young, S., & Hough, J. H. 1999, MNRAS, 304, 1
Allen, D. A., Norris, R. P., Meadows, V. S., & Roche, P. F. 1991, MNRAS, 248, 528
Antonucci, R. R. J., & Miller,J. S. 1985, ApJ, 297, 621
Armus, L., Heckman, T. M., & Miley, G. K. 1989, ApJ, 347, 727
———. 1990, ApJ, 364, 471
Axon, D. J., Hough, J. H., Young, S., & Inglis, M. 1994, Ap&SS, 216, 379
Baldwin, J. A., Phillips, M. M., & Terlevich, R. 1981, PASP, 93, 5
Barnes, J. E., & Hernquist, L. 1996, ApJ, 471, 115
Bergvall, N., Ekman, A., & Lauberts, A. 1981, A&A, 95, 266
Blanco, P. R., Ward, M. J., & Wright, G. S. 1990, MNRAS, 242, 4P
Boisson, C., & Durret, F. 1986, A&A, 168, 32
Bransford, M. A., Appleton, P. N., Heisler, C. A., Norris, R. P., & Marston, A. P. 1998, ApJ, 497, 133
Carter, D. 1984, Astron. Expr., 1, 61
Clegg, R. E. S., & Middlemass, D. 1987, MNRAS, 228, 759
Condon, J. J., Helou, G., Sanders, D. B., & Soifer, B. T. 1996, ApJS, 103, 81
Condon, J. J., Yin, Q. F., Thuan, T. X., & Boller, Th. 1998, AJ, 116, 2682
Corwin, H. G., Jr., de Vaucouleurs, A., & de Vaucouleurs, G. 1985, Southern Galaxy Catalogue (Austin: Univ. Texas)
Coziol, R., Torres, C. A. O., Quast, G. R., Contini, T., & Davoust, E. 1998, ApJS, 119, 239
Dahari, O. 1985, ApJS, 57, 643
de Grijp, M. H. K., Keel, W. C., Miley, G. K., Goudfrooij, P., & Lub, J. 1992, A&AS, 96, 389
de Robertis, M. M., & Osterbrock, D. E. 1986, ApJ, 301, 727
de Robertis, M. M., & Shaw, R. A. 1990, ApJ, 348, 421
Dopita, M. A. 1997, ApJ, 485, L41
Dopita, M. A., Heisler, C., Lumsden, S., & Bailey, J. 1998, ApJ, 498, 570
Dopita, M. A., Kewley, L. J., Heisler, C. A., & Sutherland, R. S. 2000, ApJ, in press
Dopita, M. A., Koratkar, A. P., Allen, M. G., Tsvetanov, Z. I., Ford, H. C., Bicknell, G. V., & Sutherland, R. S. 1997a, ApJ, 490, 202
Dopita, M. A., & Sutherland, R. 1995, ApJ, 455, 468
Duc, P.-A., Mirabel, I. F., & Maza, J. 1997b, A&AS, 124, 533
Durret, F., & Bergeron, J. 1988, A&AS, 75, 273
Feldman, F. R., Weedman, D. W., Balzano, V. A., & Ramsey, L. W. 1982, ApJ, 256, 427
Filipenko, A. V. 1989, in Active Galactic Nuclei, ed. D. E. Osterbrock & J. S. Miller (Dortrecht: Kluwer), 495
Fioc, M., & Rocca-Volmerange, B. 1997, A&A, 326, 950
Genzel, R., et al. 1998, ApJ, 498, 579
Heckman, T. M. 1980, A&A, 87, 152
Heckman, T. M., Butcher, H. R., Miley, G. K., & van Breugel, W. J. M. 1981, ApJ, 247, 403
Heisler, C. A., & De Robertis, M. M. 1995, AJ, 118, 2038
Heisler, C. A., Lumsden, S. L., & Bailey, J. A. 1997, Nature, 385, 700
Heisler, C. A., & Vader, J. P. 1994, AJ, 107, 35
Heisler, C. A., & Vader, J. P. 1995, AJ, 110, 87
Hill, T. L., Heisler, C. A., Sutherland, R., & Hunstead, R. W. 1999, AJ, 117, 111
Huchra, J. P. 1977, APJS, 35, 171
Inglis, M. D., Brindle, C., Hough, J. H., Young, S., Axon, S., Bailey, J. A., Ward, M. J. 1993, MNRAS, 263, 895
IRAS Catalogs and Atlases, vol. 1, Explanatory Supplement. 1988, ed. C. Beichman et al. (NASA RP−1190) (Washington, DC: GPO)
Johansson, L., & Bergvall, N. 1990, A&AS, 86, 167
Keel, W. C. 1983, ApJ, 269, 466
Kewley, L. J., Heisler, C. A., Dopita, M. A., Sutherland, R. S., Norris, R. P., Reynolds, J., & Lumsden, S. 2000, ApJ, 530, 704
Kim, D.-C., Sanders, D. B. Veilleux, Mazzarella, J. M., Soifer, B. T. 1995, ApJS, 98, 129
Kim, D.-C., Veilleux, S., & Sanders, D. B. 1998, ApJ, 508, 627
Koski, A. T. 1978, ApJ, 223, 56
Kurucz, R. L. 1992, in IAU Symp. 149, The Stellar Populations of Galaxies, ed. B. Barbuy & A. Renzini (Dordrecht: Kluwer), 225
Lauberts, A. 1982, The ESO/Uppsala Survey of the ESO(B) Atlas (Munich: Europe)
Leitherer, C., et al. 1999, ApJS, 123, 3
Lejeune, Th., Cuisinier, F., & Buser, R. 1997, A&AS, 125, 229
Lui, T. L., & Kennicutt, R. C. 1995, ApJ, 450, 547
Lutz, D., Veilleux, S., & Genzel, R. 1999, ApJ, 517, L13
Malaguti et al. 1999, A&A, 342, L41
Martin, J. M., Bottinelli, L., Dennefeld, M., & Gouguenheim, L. 1991, A&A, 245, 393
Mazzarella, J. M., & Balzano, V. A. 1986, ApJS, 62, 751
Mazzarella, J. M., Voit, G. M., Soifer, B. T., Matthews, K., Graham, J. R., Armus, L., & Shupe, D. 1994, AJ, 107, 1274
Miley, G. K., Neugebauer, G., & Soifer, B. T. 1985, ApJ, 293, L11
Miller, J. S., & Goodrich, R. W. 1990, ApJ, 355, 456
Miller, J. S., Goodrich, R. W., & Mathews, W. G. 1991, ApJ, 378, 47
Miller, J. S., & Mathews, W. G. 1972, ApJ, 172, 593
Mirabel, I. F. 1982, ApJ, 256, 120
Moshir, M., et al. 1992, Explanatory Supplement to the *IRAS* Faint Source Survey, version 2 (Pasadena: JPL) (*IRAS* FSC)
Morris, S. L., & Ward, M. J. 1985, MNRAS, 215, 57
Nilson, P. 1973, Nova Acta Regiae Soc. Sci. Upsaliensis, Series V: A, 1
Osterbrock, D. E. 1981, ApJ, 249, 4620
Osterbrock, D. E., & de Robertis, M. M. 1985, PASP, 97, 1129
Pogge, R. W., & Eskridge, P. B. 1993, AJ, 106, 140
Rafanelli, P., & Marziani, P. 1992, AJ, 103, 743
Rieke, G. H., & Low, F. J. 1972, ApJ, 176, 95
Rix, H.-W., Carleton, N. P., Rieke, G., & Rieke, M. 1990, ApJ, 363, 480
Rogers, A. W., Conroy, P., & Bloxham, G. 1988, PASP, 100, 626
Ruiz, M., Rieke, G. H., & Schmidt, G. D. 1994, ApJ, 423, 608
Rush, B., Malkan, M. A., & Spinoglio, L. 1993, ApJS, 89, 1

Sanders, D. B., & Mirabel, I. F. 1996, ARA&A, 34, 749
Sanders, D. B., Soifer, B. T., Elias, J. H., Madore, B. F., Matthews, K., Neugebauer, G., & Scoville, N. Z. 1988a, ApJ, 325, 74
Sanders, D. B., Soifer, B. T., Elias, J. H., Neugebauer, G., & Matthews, K. 1988b, ApJ, 328, L35
Schaerer, D., Contini, T., & Kunth, D. 1999, A&A, 341, 399
Scoville, N. Z., et al. 2000, ApJ, 119, 991
Shuder, J. M. 1980, ApJ, 240, 32
Shuder, J. M., & Osterbrock, D. E. 1981, ApJ, 250, 55
Simpson, C. 1998, ApJ, 509, 653
Stasińska, G., & Leitherer, C. 1996, ApJS, 107, 661
Strauss, M. A., Huchra, J. P., Davis, M., Yahil, A., Fisher, K. B., & Tonry, J. 1992, ApJS, 83, 29
Sutherland, R. S., & Dopita, M. A. 1993, ApJS, 88, 253
Taniguchi, Y., Yoshino, A., Ohyama, Y., & Nishiura, S. 1999, ApJ, 514, 660
Telesco, C. M., Wolstencroft, R. D., & Done, C. 1988, ApJ, 329, 174
Terashima, Y., Ho, L. C., Ptak, A. F., Mushotzky, R. F., Serlemitsos, P. J., Yaqoob, T., & Kunieda, H. 2000, ApJ, 533, 729
Tran, H. D. 1995, ApJ, 440, 565
Tran, H. D., Miller, J. S., & Kay, L. E. 1992, ApJ, 397, 452
van den Broek, A. C., van Driel, W., de Jong, W., Lub, J., de Grijp, M. H. K., & Goudfrooij, P. 1991, A&AS, 91, 61
Vaceli, M. S., Viegas, S. M., Gruenwald, R., & de Souza, R. E. 1997, AJ, 114, 1345
Vader, J. P., Frogel, J. A., Terndrup, D. M., & Heisler, C. A. 1993, AJ, 106, 1743
Veilleux, S. 1991, ApJ, 369, 331
Veilleux, S., Goodrich, R. W., & Hill, G. J. 1997, ApJ, 477, 631
Veilleux, S., Kim, D.-C., & Sanders, D. B. 2000, ApJ, 522, 113
Veilleux, S., Kim, D.-C., Sanders, D. B., Mazzarella, J. M., & Soifer, B. T. 1995, ApJS, 98, 171 (V95)
Veilleux, S., & Osterbrock, D. E. 1987, ApJS, 63, 295 (VO87)
Veilleux, S., Sanders, D. B., & Kim, D.-C. 1999, ApJ, 522, 139
Veron, P., Goncalves, A. C., & Veron-Cetty, M. P. 1997, A&A, 319, 52
Veron, P., Lindblad, P. O., Zuiderwijk, E. J., Veron, M. P., & Adam, G. 1980, A&A, 87, 245
Vorontsov-Velyaminov, B. A. 1959, Atlas and Catalogue of Interacting Galaxies (Moscow: Moscow State Univ.)
Vorontsov-Velyaminov, B., & Arhipova, V. P. 1963, Morphogical Catalogue of Galaxies Vol. III (Moscow: Moscow State Univ.)
———. 1968, Morphogical Catalogue of Galaxies Vol. IV (Moscow: Moscow State Univ.)
———. 1974, Morphogical Catalogue of Galaxies Vol. V (Moscow: Moscow State Univ.)
West, R. 1976, A&A, 46, 327
Whittle, M. 1985, MNRAS, 213, 33
Winkler, H. 1988, MNRAS, 234, 703
Young, S., Hough, Axon, D. J., Bailey, J. A., & Ward, M. J. 1995, MNRAS, 272, 513
Young, S., Hough, J. H., Efstathiou, A., Wills, B. J., Bailey, J. A., Ward, M. J., & Axon, D. J. 1996, MNRAS, 281, 1206
Zwicky, F. 1971, Catalogue of Selected Compact Galaxies and of Post-Eruptive Galaxies (Guemligen: Switzerland)